Title:

BBSome trains remove activated GPCRs from cilia by enabling passage through the transition zone

Authors: Fan Ye[1,2,†], Andrew R. Nager[1,†] and Maxence V. Nachury[1,2,*]

Affiliations:

[1]Department of Molecular and Cellular Physiology, Stanford University School of Medicine, CA 94305, USA

[2]Present address: Department of Ophthalmology, University of California San Francisco, CA 94143, USA

* Correspondence : Maxence.Nachury@ucsf.edu

† equal contribution

Abstract: A diffusion barrier at the transition zone enables the compartmentalization of signaling molecules by cilia. The BBSome and the small GTPase Arl6, which triggers BBSome coat polymerization, are required for the exit of activated signaling receptors from cilia, but how diffusion barriers are crossed when membrane proteins exit cilia remains to be determined. Here we found that activation of the ciliary GPCRs Smoothened and SSTR3 drove the Arl6-dependent assembly of large, highly processive and cargo-laden retrograde BBSome trains. Single-molecule imaging revealed that the assembly of BBSome trains enabled the lateral transport of ciliary GPCRs across the transition zone. Yet, the removal of activated GPCRs from cilia was inefficient because a second, periciliary diffusion barrier was infrequently crossed. We conclude that exit from cilia is a two-step process in which the BBSome/Arl6 coat first moves activated GPCRs through the transition zone before a periciliary barrier can be crossed.

One Sentence Summary: To exit cilia, activated signaling receptors must be ferried across the transition zone by the BBSome.

Introduction

Diffusion barriers establish the identity of the apical membrane in polarized epithelial cells, of the axon in neurons, of the daughter cell in budding yeast, and of cilia by impeding the lateral movement of membrane proteins (Trimble and Grinstein, 2015). The compartmentalization of cilia enables dynamic changes in ciliary composition through regulated trafficking. Upon Hedgehog pathway activation, the 7-transmembrane protein Smoothened accumulates in cilia while ciliary exit of the G protein coupled receptor (GPCR) GPR161 ensures the appropriate transduction of Hedgehog signals (Bangs and Anderson, 2017; Nager et al., 2017). While trafficking across the tight junction, the axon initial segment and the yeast bud neck involves a vesicular carrier intermediate, the mechanisms of ciliary barrier crossing remain undetermined. The ciliary diffusion barrier has been localized to the transition zone, an ultrastructural specialization between the transition fibers of the basal body and the cilium shaft (Garcia-Gonzalo and Reiter, 2012; Gonçalves and Pelletier, 2017). Three hypotheses have been advanced for crossing the transition zone (Nachury et al., 2010; Jensen and Leroux, 2017). First, the detection of vesicles inside the transition zone indicates that a vesicular carrier may transport cargoes across this barrier (Jensen et al., 2004; Chuang et al., 2015). Second, indirect evidence for lateral transport between plasma and ciliary membranes (Hunnicutt et al., 1990; Milenkovic et al., 2009) suggests that membranous cargoes laterally traverse the transition zone by active transport. Third, the regulated opening of a gate inside the transition zone may let selective cargoes move through this membranous barrier (Dyson et al., 2016).

Low-level expression recapitulates physiological ciliary trafficking dynamics

To characterize transition zone crossing by membranous cargoes, we sought a system where membrane proteins move across the transition zone in a synchronized manner. GPR161 and the

2 prototypical ciliary GPCR somatostatin receptor 3 (SSTR3) both undergo retrieval from the
3 cilium and back into the cell upon activation (Mukhopadhyay et al., 2013; Green et al., 2015).
4 GPR161, a core component of the Hedgehog pathway that couples to $G\alpha_s$, exits cilia when
5 Smoothened is activated either indirectly by Hedgehog or directly by the Smoothened agonist
6 SAG (Pal et al., 2016)(Fig. **1A**). Meanwhile, SSTR3 is a well-characterized $G\alpha_i$-coupled receptor
7 that has undergoes agonist-dependent retrieval (Nager et al., 2017; Green et al., 2015) (Fig. **1A**).
8 Consistent with previous studies on SSTR3 in hippocampal neurons (Green et al., 2015), most of
9 SSTR3 immunofluorescence was lost from neuronal cilia after 6 h treatment with the ligand
10 somatostatin-14 (sst) or the SSTR3-specific agonist L796,778 (Fig. **1B** and **S1A-C**). Similar to
11 endogenous SSTR3, ciliary exit of endogenous GPR161 and endogenous NPY2R proceeds over
12 the course of several hours (Mukhopadhyay et al., 2013; Loktev and Jackson, 2013). Signal-
13 dependent retrieval is thus a considerably slower process than signal-dependent endocytosis.

14 To dissect ciliary exit, we expressed GPCRs in mouse Inner Medullar Collecting Duct (IMCD3)
15 kidney cells, a widely used cell line for ciliary trafficking studies. GPCRs were tagged on the
16 intracellular C-terminus with a fluorescent protein (GFP or NeonGreen, NG, (Shaner et al.,
17 2013)) while a biotinylation acceptor peptide (AP) on the extracellular N-terminus combined with
18 co-expression of the biotin ligase BirA enabled pulse-chase studies with fluorescently labeled
19 monovalent streptavidin (mSA)(Howarth and Ting, 2008). When $^{AP}SSTR3^{GFP}$ under the control
20 of the EF1α promoter was stably expressed in IMCD3 cells by single integration at the FlpIn
21 locus, agonist-dependent exit of SSTR3 from cilia was undetectable. Molecular counting of GFP
22 and comparison of immunofluorescence intensities revealed that pEF1α-driven expression
23 resulted in SSTR3 levels that were an order of magnitude greater than in neurons (Fig. **1C**, top)
24 and pEF1α-driven $^{AP}SSTR3^{GFP}$ expression resulted in a near doubling of cilia length, likely due

to protein overload driving ciliary membrane expansion and compensatory axoneme growth (Fig. **1C**, bottom). To express SSTR3 at levels closer to those found in neurons, we tested a variety of weak promoters and found that an EF1α promoter lacking the TATA box (pEF1α$^{\Delta}$) produced near-endogenous ciliary levels of SSTR3 that did not alter ciliary length (Fig. **1C**). IMCD3-[pEF1α$^{\Delta}$- ^{AP}SSTR3^{NG}] cells recapitulated SSTR3 exit from cilia upon sst addition with nearly identical kinetics as in hippocampal neurons (Fig. **1B** and **S1D**). Similarly, the Hedgehog signaling-dependent exit of GPR161 was recapitulated by expressing ^{AP}GPR161^{NG3} from the δ-crystallin promoter (Fig. **1D**). pEF1α$^{\Delta}$-driven expression of NPY2R^{NG} and MCHR1^{NG} yielded low ciliary levels (Fig. **S1E**) with similar exit kinetics (Nager et al., 2017), thus demonstrating the broad applicability of low-expression promoters for studying the dynamics of ciliary GPCRs.

Calibration of the NeonGreen signal with recombinant proteins spotted on glass slides (Fig. **1E**) allowed us to estimate the absolute levels of GPCRs per cilia (Fig. **S1F-G**). Meanwhile, pulse-chase measurements with mSA-647 enabled us to specifically and quantitatively interrogate exit from cilia. Signal-dependent exit rates were close to 500 molecules per hour (Fig. **1F-G**, Movie **S1**). Further highlighting the power of AP and NG-tagged GPCRs, the increased signal-to-noise ratio endowed by direct labeling with NG or mSA647 compared to immunofluorescence (Fig. **S1H**) enabled the detection of very low abundance proteins whose presence in cilia escapes detection by traditional immunostaining techniques (Fig. **S1I**). The decreased threshold of detection of pulse-labeling ensures a more faithful visualization of exit kinetics when exit monitored by mSA647 pulse-labeling than when it was monitored by immunostaining (Fig. **1B** and **F**).

In addition, we noticed that the signal-dependent exit kinetics of ^{AP}SSTR3^{NG} were slower when monitored by direct visualization of the NG tag yielded slower than by pulse-labeling with

mSA647 (Fig. **S1J**). Even in the absence of agonist, NG fluorescence increased over time whereas mSA647 fluorescence remained constant for 6h (Fig. **S1J**). These results indicate the ciliary mSA647 signal declines faster than the ciliary NG signal because mSA647 only reports SSTR3 exit whereas the NG signal integrates SSTR3 entry and exit. We surmise that our previous attempts to assay signal-dependent exit of SSTR3 using strong promoters failed because the entry of newly-synthesized GPCRs outpaced the slow exit kinetics.

Sorting complexes for ciliary entry and exit

The low expression systems made it possible to validate the sorting complexes that carry out ciliary entry and exit. IFT-A is a complex of 6 protein with structural elements that suggest a common ancestry with coat complexes (Jékely and Arendt, 2006; van Dam et al., 2013) and IFT-A is recruited to membranes by the PI(4,5)P2-binding protein Tulp3 (Mukhopadhyay et al., 2010). Although IFT-A is often described as the central mediator of retrograde transport (Lechtreck, 2015), IFT-A and TULP3 are required for the import of many GPCRs into cilia (Mukhopadhyay et al., 2010; 2013; Loktev and Jackson, 2013; Fu et al., 2016; Hwang and Mukhopadhyay, 2017). We confirmed that Tulp3 was required for ciliary entry of SSTR3, NPY2R and MCHR1 (Fig. **2A** and **S2A-C**) and refined indirect interaction data by showing that the ciliary targeting signal of SSTR3 encoded within the third intracellular loop (i3)(Berbari et al., 2008a) is specifically and directly recognized by the purified IFT-A complex (Fig. **2B**) or by the IFT-A subunit IFT140 overexpressed in HEK cells (Fig. **S2D**). We conclude that IFT-A/Tulp3 functions as a coat adaptor complex that mediates GPCR entry into cilia by directly recognizing sorting signals (Fig. **2C**).

Consistent with the requirement for the GPCR activation sensor β-arrestin 2 in GPR161 retrieval (Pal et al., 2016), signal-dependent retrieval of SSTR3 required β-arrestin 2 (Fig. **2D** and **S2E-F**).

The BBSome, a complex of eight Bardet-Biedl Syndrome (BBS) proteins, resembles coat adaptors at the structural level and polymerizes into a planar coat upon recruitment to membranes by the GTP-bound form of the small GTPase Arl6/BBS3 (Jin et al., 2010). The function of the BBSome in entry vs. exit remains controversial. While BBSome mutants have decreased ciliary levels of the GPCRs somatostatin receptor 3 (SSTR3), melanin concentrating hormone receptor 1 (MCHR1), and NPY2R and of the polycystic kidney disease protein PKD1 (Berbari et al., 2008b; Loktev and Jackson, 2013; Su et al., 2014), GPR161, SMO and D1R fail to exit cilia in BBSome or Arl6 mutants (Zhang et al., 2011; Liew et al., 2014; Eguether et al., 2014; Yee et al., 2015; Nager et al., 2017). Finally, systematic studies find that some proteins accumulate while others are depleted from *Bbs* mutant cilia (Mick et al., 2015; Lechtreck et al., 2013; Datta et al., 2015). In our near-endogenous expression systems, deletion of Arl6 or of the candidate Arl6 activator Ift27/BBS19 or of β-arrestin2 did not reduce the steady-state ciliary levels of SSTR3 (Fig. **2A** and **S2F**). Instead, the BBSome, Arl6 and Ift27 were required for the signal-dependent retrieval of SSTR3 and GPR161 (Fig. **2D** and **S2G-H**). The carboxy-terminal tail of GPR161 ($GPR161^{Ct}$) and the third intracellular loop of SSTR3 ($SSTR3^{i3}$) directly interacted with purified BBSome (Fig. **2E**)(Jin et al., 2010), suggesting that BBSome coats sort signaling receptors through the direct recognition of cytoplasmic determinants. Since SSTR3 and GPR161 are recognized by β-arrestin 2 in a signal-dependent manner, we conclude that the signal-dependent retrieval of GPR161 and SSTR3 is jointly and directly mediated by β-arrestin 2 and the BBSome (Fig. **2F**).

Signal-dependent BBSome redistribution to the tip of cilia triggers GPCR retrieval

To characterize the mechanisms of transition zone crossing by exiting GPCRs, we first sought to determine how BBSome coats facilitate signal-dependent retrieval. The active transport of proteins inside cilia –termed intraflagellar transport– is powered by microtubule motors moving along axonemal microtubules. The movement of trains consisting of the intraflagellar transport complex B (IFT-B) can be visualized by imaging foci of the IFT-B subunit IFT88 tagged with NeanGreen traveling in the anterograde and retrograde direction inside cilia (Movie **S2**). Imaging of nematode, *Chlamydomonas* and mammalian cilia has shown that BBSome foci frequently co-move with IFT-B foci (Ou et al., 2005; Lechtreck et al., 2009; Liew et al., 2014; Williams et al., 2014), suggesting coupling between the two complexes. To follow the dynamics of the BBSome and of IFT-B during SSTR3 and GPR161 signal-dependent retrieval, we expressed ^{NG3}BBS5 or ^{NG3}IFT88 at near-endogenous levels (Fig. **3A** and **S2I**, Movie **S3**). In the absence of signaling, the BBSome and the IFT-B complex localized in a punctate pattern along the cilium (Fig. **3B**, top). Unexpectedly, SSTR3 activation led to a 4-fold enrichment of BBSome and a 2-fold enrichment of IFT-B at the tip (Fig. **3B**, bottom and **S2J-L** and Movie **S4**). Similarly, activation of the Hedgehog pathway resulted in BBSome accumulation at the ciliary tip (Fig. **3C**).

To determine whether tip enrichment of the BBSome represents a necessary intermediate in GPCR retrieval, we sought to define and manipulate the molecular mechanisms of signal-dependent tip accumulation. Since SSTR3 and Smoothened are known to couple to $G\alpha_i$ and reduce cAMP production through $G\alpha_i$-mediated inhibition of adenylate cyclases 5 and 6 (AC5/6) (Yasuda et al., 1992; Shen et al., 2013), we tested for the role of signaling downstream of $G\alpha_i$ in promoting BBSome tip enrichment (Fig. **3C-E**). Pharmacological inhibition of $G\alpha_i$ by

Pertussis toxin (PTX) blocked SAG- and sst-induced BBSome tip accumulation (Fig. **3C**). Meanwhile, inhibition of AC6 (Fig. **S2M**) or inhibition of the cAMP-dependent protein kinase (PKA) by Rp-cAMPs or by a cell permeable PKA inhibitory peptide (myr-PKI) led to BBSome tip accumulation in the absence of GPCR activation (Fig. **3C**). Furthermore, cilia-targeted PKI (Mick et al., 2015) was sufficient to redistribute BBSome to the tip (Fig. **3E**). Together with the findings of cilia-localized AC5 and AC6 (Mick et al., 2015; Masyuk et al., 2008; Kwon et al., 2010), these results suggest that activation of Smoothened and SSTR3 reduce the tonically high levels of ciliary cAMP (Moore et al., 2016) through $G\alpha_i$-mediated inhibition of AC5/6 within cilia. Since PKA was recently shown to reside and function inside cilia (Mick et al., 2015; Moore et al., 2016), we propose that PKA antagonizes the recruitment of BBSome to the tip of cilia in unstimulated cells and that activation of $G\alpha_i$-coupled GPCRs promotes BBSome tip recruitment by reducing the activity of ciliary PKA (Fig. **3D**). Importantly, pharmacological alterations of the ciliary $G\alpha_i$-PKA axis concordantly affected signal-dependent redistribution of BBSome at the tip of cilia and signal-dependent GPCR retrieval as the rates of signal-dependent retrieval of GPR161 and SSTR3 were greatly reduced by PTX (Fig. **3F-G**) and significantly accelerated by myrPKI (Fig. **3H-I**).

To further establish that BBSome tipping represents a necessary intermediate in GPCR retrieval, we sought to identify molecules that recruit the BBSome to the tip of cilia in a signal-dependent manner. The plus-end directed microtubule motor Kif7 represents a candidate tip recruitment factor because Kif7 accumulates at the tip of cilia upon Hedgehog pathway activation (Liem et al., 2009; Endoh-Yamagami et al., 2009) and appear necessary and sufficient to promote tip accumulation of the Hedgehog signaling factors Gli2 and Gli3 (He et al., 2014). Furthermore, *KIF7* is a genetic modifier of Bardet-Biedl Syndrome in human patients (Putoux et al., 2011). To

follow the behavior of Kif7 and the BBSome in live IMCD3 cells, we stably co-expressed ^{NG3}BBS5 and Kif7 fused to the red fluorescent protein mScarlet. Smoothened activation led to the correlated co-accumulated of BBS5 and Kif7 at the tip of cilia (Fig. **4A-B**). Furthermore, in the rare instances where a second spot of Kif7 was found along cilia, possibly because part of the axoneme terminates prior to the tip, a similarly intense second spot of BBS5 was observed at the same location (Fig. **4C**). Since Kif7 depletion abolished tip accumulation of the BBSome (Fig. **4D-E**), these data suggest that Kif7 may directly mediate the signal-dependent recruitment of BBSome to the tip of cilia. Congruently, Kif7 was found to co-immunoprecipitate with several BBSome subunits (Fig. **S2N**). Given that dephosphorylation of Kif7 leads to the accumulation of Kif7 at the tip of cilia (Liu et al., 2014), we considered that phosphorylation by PKA may directly antagonize Kif7 tip accumulation and the Kif7-BBSome interaction. Concordantly, PKI led to the correlated co-accumulation of BBS5 and Kif7 at the tip of cilia to the same extent as SAG (Fig. **4A-B**) and elevated cAMP levels decreased the Kif7-BBSome interaction (Fig. **4F**). Finally, Kif7 was required for signal-dependent retrieval of SSTR3 (Fig. **4G**). Together, these results suggest that signaling downstream of Smoothened and SSTR3 leads to Kif7 dephosphorylation and that the ensuing recruitment of BBSome to the tip initiates GPCR retrieval.

BBSome tip accumulation drives formation of cargo-laden retrograde trains

Analysis of ^{NG3}BBS5 and ^{NG3}IFT88 kymographs showed that anterograde BBSome trains, anterograde IFT trains and retrograde IFT trains moved processively along the length of the cilium regardless of the signaling status (Fig. **5A** and **S3A**). Yet, retrograde BBSome trains seldom reached the base of cilia in unstimulated cells because of frequent uncoupling from retrograde IFT trains (Fig. **5A-B** and **S3B)**. Activation of Smoothened or SSTR3 or inhibition of PKA all doubled the number of BBSomes per retrograde train from 10 to 20 (Fig. **5C**) and led to a

significant increase in the processivity of retrograde BBSome trains (Fig. **5D**). Meanwhile, SAG increased the number of IFT-B particles per retrograde train from 62 to 78 (Fig. **5E**). The addition of 106 BBSomes and 206 IFT-B to the tip upon SSTR3 activation (Fig. **3C and S2L**) suggests that the signal-dependent accumulation of BBSome and IFT-B at the tip drives the growth of retrograde trains by increasing the concentration of precursors at the site of assembly. Similar to the BBSome and IFT-B, Arl6 underwent signal-dependent tip accumulation (Fig. **5F**). As Arl6 was required for IFT88 tipping but not BBSome tipping (Nager et al., 2017) (Fig. **S2L**), Arl6 may recruit IFT-B particles to the tip by increasing the affinity of the BBSome for IFT-B.

PKI was sufficient to trigger tip accumulation of BBSome and Arl6 as well as the formation of large processive retrograde BBSome trains (Fig. **5C**, **F** and **S3B**), suggesting that recruitment of Arl6 and BBSome to the tip may be sufficient to initiate the assembly of large, processive retrograde IFT/BBSome trains. Because Arl6 and its candidate activator Ift27 were required for the signal-dependent formation of large processive BBSome trains (Fig. **5C-D** and **S3C**), we propose that BBSome coats polymerized upon Arl6-GTP binding become stably coupled to IFT-B trains to generate large, signal-dependent, and processive retrograde BBSome/IFT trains.

The bright and processive retrograde BBSome tracks observed upon sst addition frequently overlapped with faint tracks of SSTR3 (Fig. **5G**, Movie **S5**). No co-movement was observed between the faint BBSome trains and SSTR3 in the absence of Arl6 (Fig. **5G** and **S3D**). These observations suggest that BBSome/Arl6 coats capture cargoes and move them from tip to base of cilia upon coupling to retrograde IFT trains.

Signaling promotes the processive retrograde movement of GPCRs

In bulk fluorescence imaging, the few fluorescent GPCRs that are being trafficked tend to be obscured by the fluorescent GPCRs that remain inside cilia. To overcome the limitations inherent to ensemble imaging, we set out to visualize the molecular events that underlie GPCR retrieval at single-molecule resolution. Combining site-specific biotinylation of AP-tagged GPCRs with streptavidin-coupled quantum dots (^{SA}Qdot) enabled imaging at 2 Hz for over 20 min (compared to 30-60s when using mSA647) (Fig. **S3E**) (Ye et al., 2013). By blocking most surface-exposed biotin groups with mSA before labeling with ^{SA}Qdot, the vast majority of cilia bore no ^{SA}Qdot and cilia bearing one ^{SA}Qdot are expected to possess a single biotinylated ^{AP}GPCR (Fig. **6A**). Tracking of ^{SA}Qdot-labeled GPCRs (^{QD}GPCRs) demonstrated that their dynamics were unperturbed by ^{SA}Qdot labeling, consistent with a single valence of ^{SA}Qdot labeling per GPCR.

First, consistent with prior single-molecule tracking studies (Ye et al., 2013; Milenkovic et al., 2015), ^{QD}SSTR3 displayed a diffusive behavior in the absence of agonist (Fig. **6D**, **S4A** and Movie **S6**) and instant velocities of diffusing GPCRs were nearly identical when labeled by mSA647 or ^{SA}QD655 (Fig. **6B**). Second, congruency of exit rates between bulk imaging and ^{QD}SSTR3 imaging indicated that ^{SA}Qdot labeling did not impair exit (Fig. **6C**). Mapping the centroid of the Qdot enabled a 7 nm measurement precision (Fig. **S3F**) that resolved the lateral displacement of ^{QD}SSTR3 around the 250 nm diameter of the ciliary membrane during diffusive events (Fig. **6Ei**). Addition of sst led to ^{QD}SSTR3 undergoing frequent confinements at the base and tip as well as processive retrograde movements (Fig. **6D-E, ii-iv** and **S4B** and Movie **S7**). Persistent retrograde movements of ^{QD}SSTR3 lasting 6 s or more were strictly dependent on SSTR3 activation (Fig. **6F** and **S3G**), confirming that signaling drives formation of cargo-laden IFT/BBSome retrograde trains. This signal-dependent increase in extended processive

movements was not observed for anterograde movements (Fig. **6F**). Processive transport events did not exhibit lateral displacement (Fig. **4Eii-iv**), strongly suggesting that each cargo-laden IFT/BBSome train moves along a single axonemal microtubule. GPCRs occasionally resided for several seconds at either the tip or the base, and the frequency of confinement events –defined as residence exceeding 15s– significantly increased in the presence of sst (Fig. **6G** and **S3H**). Since processive retrograde transport events were frequently preceded by tip confinement (Fig. **6Eii** and **iv**), it is likely that tip confinement of GPCRs reflects a step of cargo capture by BBSome coats assembling at the tip. Nevertheless, ^{QD}SSTR3 exhibited retrograde movements starting at any point along the cilium (Fig. **6Eiii** and **S4B**), indicative of activated GPCRs hopping onto retrograde BBSome trains.

Similar to ^{QD}SSTR3, ^{QD}GPR161 underwent mostly diffusive behavior in unstimulated cells, and addition of SAG led to frequent retrograde processive transport events (Fig. **S4C-D**). Consistent with IFT/BBSome trains powering the retrograde transport of activated GPCRs, processive retrograde movements of ^{QD}GPR161 were absent when *Arl6* was deleted (Fig. **S4E**). The average velocity of the processive retrograde movements of ^{QD}SSTR3 was similar to previously measured values for IFT train movements (Fig. **6H**)(Ye et al., 2013), suggesting that signaling promotes coupling between cargoes and retrograde IFT trains. We conclude that activated GPR161 and SSTR3 are transported in the retrograde direction by the large, processive BBSome coats that couple to retrograde IFT trains upon GPCR activation.

Arl6 and signaling enable transition zone crossing by GPR161

The expression of ^{AP}GPCRs at near-endogenous levels enabled the ^{SA}Qdot-mediated visualization of exit from the ciliary compartment at single-molecule resolution. ^{QD}GPR161 exit followed a stereotypical sequence of processive retrograde transport, base confinement and

diffusion away from the ciliary compartment (Fig. **7A-B**, event **iii**). Surprisingly, many ^{QD}GPCRs that underwent retrograde transport and base confinement returned into the shaft of the cilium, seemingly by processive anterograde transport (Fig. **7A-B,** events **i** and **ii,** and **6C** event **iii**). During a typical pre-exit confinement event, ^{QD}GPR161 first diffused within an area of 360 nm diameter before near-complete immobilization prior to exit, suggestive of capture by an unknown machinery facilitating the final exit step (Fig. **7C, S5A** and Movie **S8-9**). Because ^{QD}GPR161 diffused within the 0.4 µm-deep focal plane after exit from the ciliary compartment, it is most likely that the GPCR moved into the plasma membrane after exit (Fig. **7C, S5A** and Movie **S8-9**). Exit event were observed at the expected frequency based on measurements of bulk exit rates, this confirms that ^{SA}Qdot labeling did not interfere with exit (Fig. **S5B**).

Unexpectedly, the position of ^{QD}GPR161 during signal-dependent base confinement events was often separate from the bulk fluorescence of GPR161^{NG3} (Fig. **8A**). Using the profile of the NeonGreen channel as a common reference (Fig. **8A-D and S5C**), we mapped the location of the most base-proximal position explored by ^{QD}GPR161 relative to the transition zone marker Cep290 and the transition fiber marker Cep164 and found that activated ^{QD}GPR161 moves into the 100 nm space between these two markers (Fig. **8A-D**). We termed the region between the 10th and 50th percentile of GPR161^{NG3} fluorescence the airlock as it defined the area visited by ^{QD}GPR161 before exit was completed. Systematic analysis of ^{QD}GPR161 position demonstrated that GPR161 enters the airlock in a signal- and Arl6-dependent manner (Fig. **8A** and **D**), thereby suggesting that large, processive BBSome trains ferry GPR161 through the transition zone and deliver it to the airlock. Finally, no extended confinement was detected before entry into the airlock and the single molecule velocities did not appreciably slow down through the transition zone (Fig. **7A** and **8E**), thus ruling out the budding of a vesicular intermediate before transition

zone crossing and suggesting instead that exiting GPCRs are actively dragged through the transition zone by IFT/BBSome trains.

Tracking ^{QD}GPR161 over a combined 70 min period of imaging in the presence of SAG revealed that the probability of ^{QD}GPR161 entering the airlock is 0.66 during a one minute interval (Fig. **S5D**). Meanwhile, the absolute exit rate (Fig. **1H**) of 0.0043 molecules/minute is equivalent to the probability of a single molecule of GPR161 experiencing exit during a one minute interval. Thus, a comparison of airlock entry frequency and ciliary exit rates revealed that less than 1% of airlock visits productively lead to exit. Meanwhile 99.3% of airlock visits are resolved by the GPCR returning into the ciliary compartment (Fig. **7Ai-ii**). Thus, while crossing the first diffusion barrier at the transition zone appears to be a prerequisite for ciliary exit, it is not sufficient to commit GPCRs for exit because a periciliary barrier blocks lateral diffusion between airlock and plasma membrane (Fig. **8F**).

Examination of the lateral position of ^{QD}GPR161 during airlock residency confirmed that GPR161 stayed within the expected 250 nm diameter of the ciliary membrane when visiting the base of cilia in unstimulated cells (Fig. **8G**). Surprisingly, the space explored by ^{QD}GPR161 during signal-dependent airlock visits increased to span a diameter of over 500 nm (Fig. **8G**), slightly larger than the diameter defined by the tip of the transition fibers (Lau et al., 2012; Yang et al., 2015; Kanie et al., 2017). The periciliary barrier thus appears to be located past the point where the transition fibers attach to the ciliary membrane.

Conclusions

We find that base confinement events precede irreversible exit from the ciliary compartment. While activation of GPR161 and SSTR3 increased their base confinement frequencies, previous

work showed that activation of Smoothened decreases its base confinement frequency (Milenkovic et al., 2015). Together with the accumulation of Smoothened in cilia of unstimulated *bbs* mutant cells (Zhang et al., 2011; 2012; Eguether et al., 2014; Goetz et al., 2017), this suggests that Smoothened is constitutively retrieved from cilia by the BBSome and that a reduction in Smoothened retrieval underlies the signal-dependent accumulation of Smoothened in cilia.

Although the idea of a periciliary diffusion barrier was initially considered (Nachury et al., 2010), the transition zone has come to be viewed as the sole diffusion barrier of the cilium in recent years (Garcia-Gonzalo and Reiter, 2012; Gonçalves and Pelletier, 2017; Jensen and Leroux, 2017). Our finding that the ciliary membrane is individualized from the plasma membrane by two successive diffusion barriers suggests the existence of an intermediate compartment located between the transition zone and a nearly impassable periciliary barrier. This intermediate compartment may correspond to the base of the ciliary pocket (Benmerah, 2013), an invagination of the plasma membrane that ensheathes the first few microns of the cilium and contacts the tip of the transition fibers at its base. Remarkably, when the receptors for insulin-like growth factor 1 (IGF1) or for transforming growth factor β (TGF-β) undergo signal-dependent exit from cilia, they transiently localize to a zone at the base of cilia that does not overlap with from axonemal markers and may correspond to the airlock. Furthermore, residence of activated IGF1R and TGF-βR at the base of cilia appears to organize downstream signaling for these two pathways (Clement et al., 2013; Yeh et al., 2013). The airlock may harbor specific lipids as both PI(4,5)P_2 and PI(3,4,5)P_3 are dynamically enriched at a zone at the base of cilia that is clearly non-overlapping from axonemal markers in mammalian cells and PI(4,5)P_2 is enriched at the ciliary pocket of trypanosomes and at the periciliary membrane compartment in nematode (Demmel et al., 2014; Jensen et al., 2015; Dyson et al., 2016). The airlock may therefore

constitute a privileged signaling locale. Finally, the existence of a second barrier explains why transition zone mutants have only mild mislocalization phenotypes and can still assemble cilia.

The finding that single GPCRs processively move down the length of the cilium and cross the transition zone without pausing (Fig. **8E**) is incompatible with the budding of a vesicular intermediate mediating crossing of the transition zone. Furthermore, since activated GPR161 only crosses the transition zone when BBSome/Arl6 coat assembly is permitted, the hypothesis that Hedgehog signaling loosens the diffusion barrier of the transition zone (Dyson et al., 2016) cannot account for GPR161 exit. Instead, our data suggests that BBSome/Arl6 coats bound to retrograde IFT trains on the axoneme-facing side and to cargoes on the membrane-facing side facilitate lateral transport through the transition zone. Thus, in contrast to all other known diffusion barriers, the transition zone is a porous barrier that allows the selective permeation of GPCRs bound to BBSome/Arl6 coats. Physical and genetic interactions between the BBSome and transition zone proteins such as Cep290 (Yee et al., 2015; Goetz et al., 2017; Zhang et al., 2014; Barbelanne et al., 2015) are in agreement with a general model where BBSome/Arl6 coats contact the transition zone during crossing. The coat adaptors AP-1 and AP-2 undergo activating conformational changes that couple membrane and cargo binding(Jackson et al., 2010), and binding to Arl6-GTP may similarly increase the affinity of the BBSome for cargoes. Taking our data into account, we propose that Arl6-GTP increases the coupling between cargoes, BBSome and IFT trains to facilitate lateral transport through the transition zone. However, the intimate details of transition zone crossing remain to be determined. In particular, the lack of precedent for selective permeation though a membrane diffusion barrier points to distinguishing biophysical features of the transition zone whose definition promises to enrich the concepts underlying diffusion barriers.

Materials and Methods

Cell line construction

For all experiments, a mouse inner medullar collecting duct IMCD3-FlpIn cell line was used (gift from Peter K. Jackson). IMCD3-FlpIn cells were cultured in DMEM/F12 (11330-057, Gibco) supplemented with 5% FBS, 100 U/mL penicillin-streptomycin, and 2 mM L-glutamine.

Cell lines expressing SSTR3, GPR161, BBS1, BBS5, and IFT88 were generated using the FlpIn System (ThermoFisher Scientific). Construction of multiple expression cassettes with low-expression promoters was conducted as described (Nager et al., 2017). Coding sequences were amplified from plasmids encoding human BBS1 and BBS5 (gifts from Val Sheffield), BirA-ER (gift from Alice Ting (Howarth and Ting, 2008), Addgene plasmid # 20856), mouse GPR161 (BC028163, MGC, Dharmacon), human NPY2R (BC075052, MGC, Dharmacon), mouse IFT88 (IOM20300, UltimateORF, Invitrogen), human MCHR1 (BC001736, MGC, Dharmacon), PACT (Pericentrin and AKAP450 centrosome-targeting domain, gift from Sean Munro (Gillingham and Munro, 2000)), mouse Kif7 (gift from Kathryn Anderson (He et al., 2014)), and mouse SSTR3 (gift from Kirk Mykytyn). BBS1, BBS5, and IFT88 were expressed by the EF1α promoter; SSTR3, NPY2R and MCHR1 the EF1α$^{\Delta}$ promoter, and GPR161 by the Crys promoter. Green Fluorescent Protein (GFP), NeonGreen (NG) (Shaner et al., 2013), mCherry, mScarlet (Bindels et al., 2017) (Addgene #85042), and TandemTomato (tdt) (Gift from Michael Davidson (Shaner et al., 2004), Addgene #54653) and an acceptor peptide for the biotin ligase BirA (AP) were used in fusion proteins. Kif7 cDNA was subcloned into a modified pCMV-based plasmid (pmScarlet-C) that was transfected into IMCD3 cells using Lipofectamine 2000, and clones were selected using Neomycin resistance. The expression level of ^{NG3}BBS5 and ^{NG3}IFT88 relative to endogenous BBS5 and IFT88 were determined by western blotting (Fig. **3A**

and **S2I**), the expression levels of exogenous SSTR3 or GPR161 compared to endogenous GPCRs were determined by measuring the intensity of ciliary fluorescence after immunostaining (Fig. **1C** and **S1B**).

CRISPR-based genome editing was done by transiently expressing Cas9 and guide RNAs (pX330, Addgene, Feng Zhang). Knockouts of *Arl6* and *Ift27* are described (Liew et al., 2014), and knockout of *Arrb2* is described (Nager et al., 2017). To generate a *Tulp3*$^{-/-}$ cell line, a guide RNA targeting the sequence ACGTCGCTGCGAGGCATCTG was used. The *Arrb1*$^{-/-}$ cell line was generated with a guide RNA targeting ACTCACCCACGGGGTCCACG. CRISPR-modified clones were isolated by limited dilution, and verified by western blotting for the disrupted gene product. To confirm gene editing, the modified genomic locus was isolated used using the ThermoFisher CloneJET PCR cloning kit.

Low Expression Promoters

Cloning of constructs with low expression promoters was done as described (Nager et al., 2017). Briefly, an *NsiI* restriction cloning site was inserted by site directed mutagenesis before the EF1α promoter in pEF5B/FRT (Nager et al., 2017). The EF1α promoter was then excised by NsiI and SpeI, and replaced by either the UbC, thymidine kinase (TK), EF1α$^{\Delta}$, CMV$^{\Delta}$, or a minimal chicken lens δ-crystallin promoter (Morita et al., 2012; Ferreira et al., 2011; Kamachi and Kondoh, 1993). The UbC promoter was cloned from pLenti6/UbC/V5-Dest (Cat. #V49910, ThermoFisher Scientific). The thymidine kinase promoter was from pRL TK (Cat. #E2241, Promega). EF1α$^{\Delta}$ consists of a TATA-less EF1α promoter from pEF5/FRT/V5-Dest (Cat. #V602020, ThermoFisher Scientific) wherein the TATA box sequence, TATAA, was mutated to TCCCC. CMV$^{\Delta}$ was designed after the CMV(Δ6) promoter (Morita et al., 2012), and was cloned from pcDNA3.1 (Cat. #V79020, ThermoFisher Scientific). The chicken lens δ-

crystallin promoter was cloned from a pGL3-8xGli-Firefly-Luciferase plasmid (gift from Phil Beachy).

Hippocampal Neurons

Rat hippocampal neurons were dissected from postnatal day 0 or 1 rat pups and plated on poly-D-lysine-coated 12 mm #0 cover glass. Neurons were cultured in Neurobasal medium with serum-free B27 and Gibco GlutaMAX. Neurons were identified by nuclear NeuN staining in immunofluorescence studies.

Transfection

siRNAs were reverse-transfected by Lipofectamine RNAiMAX. Briefly, detached cells were plated with the transfection reagent in Optimem. Cells were then grown for 48 h before 24 h starvation and subsequent imaging. Control (Cat. #D-001210-04-05), BBS1 (Cat. #D-019180-03), BBS2 (Cat. #D-010080-02) and BBS4 (Cat. #D-054691-03) were from Dharmacon, and the Kif7 siRNA (Cat. #GS16576) and matched control (Cat. #1027280) were from Qiagen. siRNA targeting Arl6 was described (Jin et al., 2010).

Pharmacology

Small molecules were added at the following concentrations and for the indicated pre-treatment times unless otherwise indicated: ACQ090 (20 μM), IBMX (500 μM, 30 min pre-incubation), L796,778 (Merck (Rohrer et al., 1998), 10 μM), PKI (50 μM, 40 min pre-incubation), PTX (10 ng/mL, 16 h pre-incubation), Rp-cAMPS (10 μM, 2 h pre-incubation), SAG (200 nM), Somatostatin (10 μM), SQ225 (500 μM, 40 min pre-incubation).

2 Antibodies and Affinity Reagents

3 The following antibodies were used: AC3 (sc-588, Santa Cruz Biotechnology), acetylated
4 tubulin (6-11-B, Sigma-Aldrich), Arl6 (Jin et al.; 2010), β-Arrestin1 (15361-1-AP, Proteintech
5 Group), β-Arrestin2 (10171-1-AP, Proteintech Group), BBS5 (14569-1-AP, Proteintech Group),
6 BBS9 (HPA021289, Sigma-Aldrich), Centrin (20H5, Millipore), Cep164 (gift from Tim Stearns),
7 Cep290 (gift from Sophie Saunier), c-Myc (sc-40, Santa Cruz Biotechnology), GFP (A11122,
8 Invitrogen), GPR161 (gift from Saikat Mukhopadhyay), IFT139 (gift from Pamela Tran), IFT140
9 (17460-1-AP, Proteintech Group), NeuN (MAB377, Millipore), Ninein (gift from Michel
10 Bornens), Phospho-p44/42 MAPK Erk1/2 Thr202/Tyr204 (4370, Cell Signaling Technologies),
11 SSTR3 (sc-11617, Santa Cruz Biotechnology), and TULP3 (gift from John Eggenschwiler).
12 Biotinylated SSTR3 and GPR161 were detected using Alexa647-labeled monovalent
13 streptavidin (Ye et al., 2013).

14

15 Protein-Protein Interaction Assays

16 IFT-A was purified through a LAP tag on the N-terminus of IFT43 as described (Nachury,
17 2008). Briefly, IMCD3-[pEF1α-^{LAP}IFT43] were harvested and lysed, and the IFT-A complex
18 was captured by GFP immunoaffinity and eluted with the TEV protease. GST and GST-SSTR^{i3}
19 fusion proteins were purified from *E.coli*, and used for interaction assays as described (Jin et al.,
20 2010).

21 The interaction of ^{GFP}Kif7 with ^{Myc}BBS1 was assayed by co-transfection/co-IP. HEK293
22 cells were forward transfected in a 6-cm plate with plasmids expressing ^{GFP}Kif7 and either
23 ^{Myc}RFP or a Myc-tagged BBSome subunit. After two days, cells were washed and treated with
24 media containing either IBMX or DMSO for 30 min. Cells were then trypsinized, pelleted and
25 cleaned in a flacon tube, and lysed for 10 min with cold CoIP buffer (50 mM Tris pH 7.4, 150

mM NaCl, 1% Triton X-100, 1 mM DTT, 1 mM AEBSP, 800 nM Aprotonin, 15 μM E-64, 10 mg/ml Leupeptin, 10 mg/ml Pepstatin A, 10 mg/ml Bestatin). The resulting lysates were then centrifuged for 15 min, concentration-matched, and then added to anti-GFP antibody coupled beads in CoIP buffer. The beads were rotated for 20 min at 4°C, pelleted and washed with CoIP buffer 4 times, and eluted by boiling in SDS-PAGE loading buffer.

Absolute quantification of cilia-localized markers

In Fig. **1C**, the number of ^{AP}SSTR3^{GFP} molecules per cilium resulting from expression driven by the EF1α, UBC, TK, EF1α$^{\Delta}$, and CMV$^{\Delta}$ promoters was estimated by comparison to a viral particle containing exactly 120 GFP molecules (Breslow et al., 2013). As ciliary GFP was not detectable by direct imaging of the IMCD3-[pCrys-^{AP}SSTR3^{GFP}] line, immunostaining for GFP was used to amplify the fluorescent signal and compare to immunostained GFP in IMCD3-[pEF1α$^{\Delta}$ -SSTR3^{GFP}] cells. To estimate the number of SSTR3 molecules per hippocampal neuron, hippocampal neurons and IMCD3-[^{AP}SSTR3^{GFP}] cells using the aforementioned promoters were compared by SSTR3 immunostaining. The epitope recognized by the SSTR3 antibody (sc-11617, Santa Cruz Biotechnology) is identical between rat and mouse (Santa Cruz Biotechnology, personal communication).

For quantification of NeonGreen-tagged proteins including ^{AP}SSTR3^{NG}, ^{AP}GPR161^{NG3}, ^{NG3}BBS5, and ^{NG3}IFT88, ciliary molecules were quantified using single NeonGreen trimers (NG3) as a calibrator (Prevo et al., 2015). NG3 protein was recombinantly expressed in *E. coli*, and purified by nickel affinity. The purified protein was then sparsely immobilized on a 18x18 mm coverslip for imaging on a DeltaVision microscope. Imaging was done in Invitrogen Live Cell Imaging Solution (Cat. #A14291DJ). To confirm that fluorescent foci originate from a single NG3, we confirmed that fluorescence was lost by photobleaching in three discrete steps (Fig. **1E**).

The mean fluorescent intensity from over 1257 molecules was then used to estimate the number of NeonGreen-tagged molecules in cilia.

To quantify the absolute number of ciliary proteins, serum staved live IMCD3 cells were imaged in Invitrogen Live Cell Imaging Solution (Cat. #A14291DJ) with the same exposure setting as used in single NG3 fluorescent quantification. Therefore,

$$N_{cilia} = (F_{cilia_NG} - F_{background}) / ((F_{NG3} / n) * R_{expression})$$

Where N_{cilia} is the absolute number of ciliary protein, F_{cilia_NG} is the total ciliary fluorescence detected from NG or NG3 labeled proteins, $F_{background}$ is the background fluorescence measured in the adjacent area. F_{NG3} is the fluorescent intensity of a single NG3 protein, n determined by the single or triple NG tag was used. For example, n = 3 for ^{AP}SSTR3^{NG} and n=1 for GPR161^{NG3}. $R_{expression}$ is the abundance ratio between the NeonGreen-tagged form of a given protein and the total amount of that protein in cilia. For pEF1α-^{NG3}BBS5 and pEF1α-^{NG3}IFT88, $R_{expression}$ = 0.55 and 0.51 respectively, which were measured by western blotting (Fig. **3A** and **S2I**). For pEF1α$^{\Delta}$-^{AP}SSTR3^{NG}, $R_{expression}$ = 1 since IMCD3 cells do not express SSTR3. For ^{AP}GPR161^{NG3}, $R_{expression}$ could not be directly measured because tagging of GPR161 at the C-terminus (e.g. in GPR161^{NG3}) interferes with recognition by the anti-GPR161 antibody developed by Mukhopadhyay and colleagues (Mukhopadhyay et al., 2013). We thus utilized ^{AP}GPR161 as an intermediate calibrator between ^{AP}GPR161^{NG3} and endogenous GPR161. A plasmid encoding pCrys-^{AP}GPR161 was transfected into IMCD3 cells and the relative expression levels of transiently expressed ^{AP}GPR161 and stably expressed ^{AP}GPR161^{NG3} were measured by mSA647 pulse-labeling.

$$R_{AP.GPR161.NG3:AP.GPR161} = F_{mSA.Gpr161.NG3} / F_{mSA.GPR161}$$

Where $R_{AP.GPR161.NG3:AP.GPR161}$ is the ratio between stably expressed $^{AP}GPR161^{NG3}$ and transiently expressed $^{AP}GPR161$ in cilia, $F_{mSA.GPR161}$ is the ciliary fluorescence signal measured by mSA647 labeling of transiently expressed $^{AP}GPR161$, and $F_{mSA.Gpr161.NG3}$ is the ciliary fluorescence signal measured by mSA647 labeling of stably expressed $^{AP}GPR161$.

The relative ciliary expression levels of endogenous GPR161 and $^{AP}GPR161$ were measured by anti-GPR161 antibody.

$$R_{endoGPR161:AP.GPR161} = F_{Ab} / (F_{Ab+AP.GPR161} - F_{Ab})$$

Where $R_{endoGPR161:\ AP.GPR161}$ is the ratio between endogenous GPR161 and transiently expressed $^{AP}GPR161$ in cilia, F_{Ab} is the ciliary fluorescence signal measured by immunofluorescence of untransfected cells with the anti-GPR161 antibody and $F_{Ab+AP.GPR161}$ is the ciliary fluorescence signal measured by immunofluorescence of cells transiently expressing with $^{AP}GPR161$ with the anti-GPR161 antibody.

Therefore,

$$N_{AP.GPR161.NG3} = (F_{cilia.NG} - F_{background}) / F_{NG3}$$

$$R_{endoGPR161:AP.GPR161.NG3} = R_{endoGPR161:AP.GPR161} / R_{AP.GPR161.NG3:AP.GPR161}$$

$$N_{endoGPR161} = N_{AP.GPR161.NG3} / R_{endoGPR161:AP.GPR161.NG3}$$

$$R_{expression} = N_{AP.GPR161.NG3} / (N_{AP.GPR161.NG3} + N_{endoGPR161})$$

Where $R_{endoGPR161:AP.GPR161.NG3}$ is the ciliary abundance ratio between endogenous GPR161 and stably expressed $^{AP}GPR161^{NG3}$; $N_{endoGPR161}$ and $N_{AP.GPR161.NG3}$ are the absolute number of endogenous GPR161 and stably expressed $^{AP}GPR161^{NG3}$ in cilia; F_{cilia_NG} is the total ciliary fluorescence detected in the green channel from $^{AP}GPR161^{NG3}$; $F_{background}$ is the background fluorescence measured in the adjacent area; F_{NG3} is the fluorescent intensity of a single NG3 protein; $R_{expression}$ is the ciliary abundance ratio between stably expressed $^{AP}GPR161^{NG3}$ and total GPR161. Using the above strategy, we determined that:

$$N_{AP.GPR161.NG3} = 1226$$

$$N_{endoGPR161} = 949$$

$$R_{expression} = 0.56$$

Bulk GPCR Exit Assays

Bulk measurements of GPCR exit were done as described previously (Nager et al., 2017). Briefly, to measure SSTR3 exit, cell expressing $^{AP}SSTR3^{NG}$ were pulse-labeled with Alexa647-labeled mSA, washed, and imaged on a DeltaVision microscope following addition of somatostatin. For each time point, the integrated Alexa647 fluorescence density was measured

using ImageJ. The cilia-adjacent fluorescence was subtracted as the background, and a mathematical photobleaching correction was applied:

$$F_{cilia} = (F_{SA647_measured} / F_{SA647_1}) + (1 - e^{-\lambda * (n-1)})$$

Where λ is the photobleaching decay constant, n is the number of images taken, $F_{SA647_measured}$ is the integrated SA647 fluorescence measured for image 'n', F_{SA657_1} is the measurement for the first time point, and F_{cilia} is the reported fluorescence. In this equation, F_{cilia} is reported in Relative Fluorescence Units (RFUs).

$^{AP}GPR161^{3NG}$ was assayed similarly except that quantifications were done by NG fluorescence intensity using the following equation:

$$GPR161_{cilia} = (F_{NG3_n} / F_{NG3_1}) * (\mu_{F_NG3_Cilia} * \mu_{F_NG3})$$

Where $GPR161_{cilia}$ is the number of GPR161 molecules in the cilium, F_{NG3_n} is the photobleaching-corrected integrated NG fluorescence measured for image 'n', F_{NG3_1} is the measurement for the first time point, $\mu_{F_NG3_Cilia}$ is the mean integrated NG fluorescence from a population of $^{AP}GPR161^{NG3}$ cilia, and μ_{F_NG3} is the mean integrated green fluorescence from individual NG3 molecules.

To measure the exit rate of SSTR3 and GPR161 in the first 2h after adding agonist (Fig **1F-G**),

$$R_{exit/h} = N_{cilia} * (F_{cilia_1} - F_{cilia_2h}) / (2 * F_{cilia_1})$$

Where $R_{exit/h}$ is the number of SSTR3 or GPR161 that exited cilia per hour, F_{cilia_1} is the background corrected ciliary fluorescent intensity before adding agonist, F_{cilia_2h} is the background corrected ciliary fluorescent intensity after 2h of agonist treatment, N_{cilia} is the absolute number of SSTR3 or GPR161 molecules in cilia as described in previous section.

To assess significant differences in GPCR removal, we used multiple regression. First, raw data was linearly fitted ($F_{cilia} = m * time + c$). Conditions were then compared using a z-statistic:

$$z = (m_1 - m_2) / (se_{1,2})$$

Where m_1 and m_2 are the fitted slopes for two experiments, and $se_{1,2}$ is the propagated standard error of the slopes:

$$se_{1,2} = sqrt(s_{m1}^2 + s_{m2}^2)$$

Where s_{m1} and s_{m2} are the standard deviations for m_1 and m_2, respectively. Z-statistics were converted to p-values for statistical interpretation.

Fixed Imaging

In a 24-well plate, 50,000 to 100,000 cells were seeded on Fisherbrand acid-washed cover glass (12 mm #1.5). Cells were grown for 24 h, and then starved for 16-24 h in 0.2% FBS media prior to experimental treatment. After treatment, cells were fixed with room-temperature 4%

2 paraformaldehyde in phosphate buffer saline (PBS) for 5 min, extracted in -20°C methanol for 5
3 min, permeabilized in PBS containing 0.1% Triton-X100, 5% normal donkey serum (017-000-
4 121, Jackson Immunoresearch Labs), and 3% bovine serum albumin (BP1605-100,
5 ThermoFisher Scientific) for 30 min, and subsequently immunolabeled for imaging. Briefly, cells
6 were incubated with primary antibodies for 1 h, washed three times with PBS, incubated with
7 dye-coupled secondary antibodies (Jackson Immunoresearch Labs) for 30 min, washed two times
8 with PBS, stained with Hoechst DNA dye, washed twice more with PBS, and mounted on slides
9 using Fluoromount-G (Electron Microscopy Sciences). Cells were then imaged on a DeltaVision
10 system. In most experiments, cilia closest to the cover slip were imaged (ventral cilia) as these cilia
11 often lay perpendicular to the objective and within a single focal plan. In select cases, cilia
12 pointing away from the coverslip (dorsal cilia) were imaged as to reduce background
13 fluorescence. To do so, a Z-stack of images with 0.3-μm separation was collected and
14 deconvolved using SoftWoRx 6.0.
15
16 Live-Cell Imaging
17 400,000 cells were seeded on acid-washed 25 mm cover glass (Electron Microscopy
18 Sciences) in a 6 cm dish. After 24 h of growth, cells were starved for 16 h and transferred to the
19 DeltaVision stage for imaging at 37 °C inside an environmental chamber. Cells were imaged in
20 DMEM/F12 media, with HEPES and no phenol red and 0.2% FBS (11039-021, Gibco). For all
21 >1 h imaging experiments, the imaging chamber was overlaid with a petri dish containing a
22 moist towel to maintain the imaging volume and pH. To accurately measure removal of
23 ^{AP}SSTR3^{NG}, the biotinylated AP tag of SSTR3 was pulse-labeled with Alexa647-labeled
24 monovalent streptavidin (SA647) for 5 min as described (Ye et al., 2013).
25

2 DeltaVision microscope

3 All imaging was conducted on an Applied Precision DeltaVision equipped with a PlanApo
4 60×/1.40 numerical aperture (NA) oil objective lens and a PlanApo 60×/1.49 NA total internal
5 reflection microscopy (TIRF) oil objective lens (Olympus) and a 488 nm laser from DeltaVision
6 Quantifiable Laser Module (QLM), and images were captured with a sCMOS camera with the
7 pixel size of 0.1077 μm (Applied Precision, GE).

8

9 Kymograph Analysis and Processivity

10 To analyze intraciliary trafficking, IFT88 and BBS5 proteins were genetically labeled with
11 NG3 and rapidly imaged with TIRF (4 Hz) for short time periods (30-60 s). TIRF illumination
12 reduced nonciliary (background) fluorescence, permitting visualization of dim trains. The
13 resulting movies were analyzed by ImageJ for generating kymographs. KymographClear and
14 KymographDirect (Mangeol et al., 2016) were used to deconvolve anterograde from retrograde
15 trains for measuring train frequency and relative intensities (e.g. Fig. **5A**) whereas Multi
16 Kymograph was used for unaltered presentation (e.g. Fig. **5B**).

17 The processivity of IFT-B or BBSome trains along axonemal microtubules was defined as
18 the duration for which a fluorescent focus of IFT88 or BBS5 unidirectionally moved along the
19 the cilium at a rate expected for kinesin or dynein-mediated transport (0.3-0.6 μm /s). Only
20 events occurring for longer than 3 seconds were considered. Measurements were made from
21 kymographs of ^{NG3}IFT88, ^{NG3}BBS5, or ^{mCherry}IFT88 and ^{NG3}BBS5. Briefly, kymographs were
22 visualized in ImageJ, and lines were drawn along the long axis of the cilium ("the leg") and the
23 processive movement ("the hypotenuse"). Comparison of the cilia long axis and the hypotenuse
24 was used to quantify the processivity and velocity of a IFT or BBS-containing train.

25

2 Quantification of IFT/BBS trains

3 To estimate the number of IFT88 or BBS5 molecules per train, the total NG3 fluorescence
4 along the ciliary axoneme was first divided by the number of trains:

5

6 $T_{RFU_mean} = \mu_{RFU_NG3_axoneme} / N_{train}$

7

8 Where T_{RFU_mean} is the estimated ^{NG3}IFT88 or ^{NG3}BBS5 fluorescence of a single train,
9 $\mu_{RFU_NG3_axoneme}$ is the mean integrated fluorescence along the axonemes of several cilia
10 (excluding the base and the tip), and N_{train} is the number of trains counted by kymograph analysis
11 in the cilia when $\mu_{RFU_NG3_axoneme}$ was measured. To increase measurement precision for
12 calculating $\mu_{RFU_NG3_axoneme}$, cilia were imaged by epifluorescence rather than TIRF illumination
13 as the TIRF field did not reproducibly illuminate cilia from different cells. T_{RFU_mean} was then
14 used to calculate the absolute number of IFT88 or BBS5 molecules per train by using the NG3
15 standard described above (see "Absolute quantification of cilia-localized markers"):

16

17 $T_{labeled_abs} = T_{RFU_average} / \mu_{F_NG3}$

18

19 Where $T_{labeled_abs}$ is the average number of labeled molecules per train, and μ_{F_NG3} is the
20 previously-measured mean fluorescence of a single NG3. As $T_{labeled_abs}$ does not account for
21 unlabeled IFT88 or BBS5 within a train, a correction must be applied that relates the ratio of
22 unlabeled to labeled molecules in the cell:

23

24 $T_{abs} = T_{labeled_abs} * ((W_{NG3} + W_{endogenous}) / W_{NG3})$

25

Where T_{abs} is the number of IFT88 or BBS5 molecules per train, and W_{NG3} and $W_{endogenous}$ are the integrated intensities of western blot bands for NG3-tagged and endogenous molecules using antibodies against mouse IFT88 or BBS5 (Fig. **3A** and **S2I**). T_{abs} was used to calculate the number of molecules in an anterograde ($T_{abs_anterograde}$) versus retrograde ($T_{abs_anterograde}$) train:

$$T_{abs} = (f_{anterograde} * T_{abs_anterograde} + f_{retrograde} * T_{abs_retrograde}) / (f_{anterograde} + f_{retrograde})$$

Where $f_{anterograde}$ and $f_{retrograde}$ are the frequency of either anterograde or retrograde trains. Using KymographClear analysis on ^{NG3}IFT88, we measure $f_{anterograde}$ = 21.4 trains/min and $f_{retrograde}$ = 18.5 trains/min. $T_{abs_anterograde}$ and $T_{abs_retrograde}$ can now be solved using the size ratio (R_T) of anterograde versus retrograde trains:

$$R_T = \mu_{RFU_T_anterograde} / \mu_{RFU_T_retrograde}$$

Where $\mu_{RFU_T_anterograde}$ and $\mu_{RFU_T_retrograde}$ are the mean NG3 intensity of anterograde or retrograde trains. By KymographClear analyses, R_T = 1.69 for ^{NG3}IFT88, and R_T = 1.78 for ^{NG3}BBS5. Relating $T_{abs_anterograde}$ to $T_{abs_retrograde}$:

$$T_{abs_anterograde} = T_{abs_retrograde} * R_T$$

One can calculate the number of IFT88/BBS5 particles in anterograde and retrograde trains:

$$T_{abs_anterograde} = (f_{anterograde} + f_{retrograde}) * T_{abs} / (f_{anterograde} + f_{retrograde} / R_T)$$

$$T_{abs_retrograde} = (f_{anterograde} + f_{retrograde}) * T_{abs} / (f_{anterograde} * R_T + f_{retrograde})$$

Line scan and tipping quantification

The longitudinal fluorescence intensities of BBS5, IFT88, SSTR3 and GPR161 were measured in ImageJ by a Plot Profile of a 5-pixel-wide line along the long axis of the cilium. To average data from multiple cilia, Pixel Intensities were assigned a length-percent with 0% referring to the base, and 100% referring to the tip. Values were then grouped into 5% bins and averaged. Bin means were then averaged across multiple cilia and plotted (e.g. Fig. **3B**).

To quantify ^{NG3}BBS5 tipping, a 5x7 pixel box was centered at the cilium tip, and the integrated fluorescence intensity within the box was measured by ImageJ. The resulting values were background corrected by subtracting the fluorescence immediately adjacent to the cilium. The values from multiple ciliary tips were averaged, and then converted to absolute numbers of BBS5 particles using the NG3 calibration.

Single-molecule labeling with ^{SA}Qdot

Molecules of SSTR3 or GPR161 present on the surface of IMCD3-[pEF1α$^{\Delta}$-^{AP}SSTR3^{NG}] and IMCD3-[pCrys-^{AP}GPR161^{NG3}] cells were labeled with ^{SA}Qdot through the affinity of streptavidin for the extracellular biotinylated AP tag. Both cells lines express an ER-targeted BirA ligase that biotinylates the N-terminal AP tag of each GPCR (Nager et al., 2017; Howarth and Ting, 2008). Single GPCR labeling was achieved through a blocking strategy. First, to block surface-exposed biotinylated receptors, cells were washed with PBS (3 times), and then incubated with 10 nM mSA for 15 min. Cells were washed with PBS (3 times), and incubated with 1 nM ^{SA}Qdot (ThermoFisher Scientific) solution for 15 min. As the ^{SA}Qdot only binds to receptors newly arrived at the surface during the 15 min of labeling, this approach labels very few

receptors. Lastly, cells were washed with PBS (3 times), and transferred to imaging media (DMEM/F12, HEPES, no phenol red media; 11039-021, Gibco) with 0.2% FBS and 1 μM biotin to block unbound Streptavidin on ^{SA}Qdot.

Qdot-labeled SSTR3 and GPR161 molecules exited the cilium at rates congruent with bulk imaging (Fig. **1F-G**). By counting the number of ^{QD}SSTR3 per cilia after 2 h treatment with vehicle or sst (Fig. **6C**), we determined that sst resulted in the loss of 25% of cilia-localized Qdots, consistant with the SSTR3 exit rate measured by bulk fluorescence (Fig. **1F**). As a second test, the frequencies of ^{QD}GPR161 exit events captured by live imaging matched the frequencies predicted from imaging the decrease in bulk fluorescence of GPR161^{NG3} (Fig. **S5B**).

Qdot localization and analysis

To monitor single receptor trafficking, cilia bearing one Qdot were imaged on the Deltavision microscope at 2 Hz for 5 to 20 min. Cilia were identified by the NG signal from the C-terminal NG and NG3 tags. The centroid of ^{SA}QD-labeled single SSTR3 and GPR161 were mapped as described (Sage et al., 2005). The localization precision of Qdot was measured as described (Deschout et al., 2014).

Processivity, residence, and confinement frequencies are based on kymograph analyses (examples shown in Fig. **S4**). Processive ^{QD}GPCR movements were defined as consecutive frames were a Qdot moved longitudinally along the ciliary axoneme. To distinguish motor-driven from diffusive events, only processive motions that extend for at least 6 consecutive frames (Fig **S3G**) or 10 consecutive frames (Fig. **6F**) are plotted. Residence at the base and tip was operationally defined as residing at the basal or distal 10% length of the cilium for longer than 2.5 seconds (Fig. **6G**). As freely diffusing receptors occasionally remain at the cilia base or tip for more than 2.5

seconds, confinement was defined by a more stringent criterion of events lasting longer than 15 seconds (Fig. **6G**).

The most base-proximal position (x_{base}, y_{base}) of ^{QD}GPR161 was mapped on a coordinate system established by the profile of ciliary GPR161^{NG3} (Fig. **8A, C-D** and **G**). The same approach was applied to map the immunofluorescence intensity center of Cep290 and Cep164 (Fig. **8B** and **D**). Airlock visits were defined as events where the QDot centroid crossed the 50th percentile of NG intensity in the GPR161^{NG} longitudinal scan profile (Fig. **8D**).

Box Plots

All box plots display the second, third, and fourth quartiles along with whiskers that represent values within the 1.5x the interquartile range. Outliers exceeding the whiskers are plotted as points.

References and Notes

Bangs, F., and K.V. Anderson. 2017. Primary Cilia and Mammalian Hedgehog Signaling. *Cold Spring Harb Perspect Biol*. 9:a028175. doi:10.1101/cshperspect.a028175.

Barbelanne, M., D. Hossain, D.P. Chan, J. Peränen, and W.Y. Tsang. 2015. Nephrocystin proteins NPHP5 and Cep290 regulate BBSome integrity, ciliary trafficking and cargo delivery. *Hum Mol Genet*. 24:2185–2200. doi:10.1093/hmg/ddu738.

Benmerah, A. 2013. The ciliary pocket. *Curr Opin Cell Biol*. 25:78–84. doi:10.1016/j.ceb.2012.10.011.

Berbari, N.F., A.D. Johnson, J.S. Lewis, C.C. Askwith, and K. Mykytyn. 2008a. Identification of Ciliary Localization Sequences within the Third Intracellular Loop of G Protein-coupled Receptors. *Mol Biol Cell*. 19:1540–1547. doi:10.1091/mbc.E07-09-0942.

Berbari, N.F., J.S. Lewis, G.A. Bishop, C.C. Askwith, and K. Mykytyn. 2008b. Bardet-Biedl syndrome proteins are required for the localization of G protein-coupled receptors to primary cilia. *Proc Natl Acad Sci USA*. 105:4242–4246. doi:10.1073/pnas.0711027105.

Bindels, D.S., L. Haarbosch, L. van Weeren, M. Postma, K.E. Wiese, M. Mastop, S. Aumonier, G. Gotthard, A. Royant, M.A. Hink, and T.W.J. Gadella. 2017. mScarlet: a bright monomeric red fluorescent protein for cellular imaging. *Nat Methods*. 14:53–56. doi:10.1038/nmeth.4074.

Breslow, D., E.F. Koslover, F. Seydel, A.J. Spakowitz, and M.V. Nachury. 2013. An in vitro assay for entry into cilia reveals unique properties of the soluble diffusion barrier. *J Cell Biol*. 203:129–147. doi:10.1083/jcb.201212024.

Chuang, J.Z., Y.-C. Hsu, and C.H. Sung. 2015. Ultrastructural visualization of trans-ciliary rhodopsin cargoes in mammalian rods. *Cilia*. 4:4. doi:10.1186/s13630-015-0013-1.

Clement, C.A., K.D. Ajbro, K. Koefoed, M.L. Vestergaard, I.R. Veland, M.P.R. Henriques de Jesus, L.B. Pedersen, A. Benmerah, C.Y. Andersen, L.A. Larsen, and S.T. Christensen. 2013. TGF-β signaling is associated with endocytosis at the pocket region of the primary cilium. *Cell Rep*. 3:1806–1814. doi:10.1016/j.celrep.2013.05.020.

Datta, P., C. Allamargot, J.S. Hudson, E.K. Andersen, S. Bhattarai, A.V. Drack, V.C. Sheffield, and S. Seo. 2015. Accumulation of non-outer segment proteins in the outer segment underlies photoreceptor degeneration in Bardet-Biedl syndrome. *Proc Natl Acad Sci U S A*. 112:E4400–9. doi:10.1073/pnas.1510111112.

Demmel, L., K. Schmidt, L. Lucast, K. Havlicek, A. Zankel, T. Koestler, V. Reithofer, Pietro de Camilli, and G. Warren. 2014. The endocytic activity of the flagellar pocket in Trypanosoma brucei is regulated by an adjacent phosphatidylinositol phosphate kinase. *J Cell Sci*. 127:2351–2364. doi:10.1242/jcs.146894.

Deschout, H., F. Cella Zanacchi, M. Mlodzianoski, A. Diaspro, J. Bewersdorf, S.T. Hess, and K.

Braeckmans. 2014. Precisely and accurately localizing single emitters in fluorescence microscopy. *Nat Methods*. 11:253–266. doi:10.1038/nmeth.2843.

Dyson, J.M., S.E. Conduit, S.J. Feeney, S. Hakim, T. DiTommaso, A.J. Fulcher, A. Sriratana, G. Ramm, K.A. Horan, R. Gurung, C. Wicking, I. Smyth, and C.A. Mitchell. 2016. INPP5E regulates phosphoinositide-dependent cilia transition zone function. *J Cell Biol*. 216:247–263. doi:10.1083/jcb.201511055.

Eguether, T., J.T. San Agustin, B.T. Keady, J.A. Jonassen, Y. Liang, R. Francis, K. Tobita, C.A. Johnson, Z.A. Abdelhamed, C.W. Lo, and G.J. Pazour. 2014. IFT27 links the BBSome to IFT for maintenance of the ciliary signaling compartment. *Dev Cell*. 31:279–290. doi:10.1016/j.devcel.2014.09.011.

Endoh-Yamagami, S., M. Evangelista, D. Wilson, X. Wen, J.-W. Theunissen, K. Phamluong, M. Davis, S.J. Scales, M.J. Solloway, F.J. de Sauvage, and A.S. Peterson. 2009. The mammalian Cos2 homolog Kif7 plays an essential role in modulating Hh signal transduction during development. *Curr Biol*. 19:1320–1326. doi:10.1016/j.cub.2009.06.046.

Ferreira, J.P., R.W.S. Peacock, I.E.B. Lawhorn, and C.L. Wang. 2011. Modulating ectopic gene expression levels by using retroviral vectors equipped with synthetic promoters. *Syst Synth Biol*. 5:131–138. doi:10.1007/s11693-011-9089-0.

Fu, W., L. Wang, S. Kim, J. Li, and B.D. Dynlacht. 2016. Role for the IFT-A Complex in Selective Transport to the Primary Cilium. *Cell Rep*. 17:1505–1517. doi:10.1016/j.celrep.2016.10.018.

Garcia-Gonzalo, F.R., and J.F. Reiter. 2012. Scoring a backstage pass: mechanisms of ciliogenesis and ciliary access. *J Cell Biol*. 197:697–709. doi:10.1083/jcb.201111146.

Gillingham, A.K., and S. Munro. 2000. The PACT domain, a conserved centrosomal targeting motif in the coiled-coil proteins AKAP450 and pericentrin. *EMBO Rep*. 1:524–529. doi:10.1093/embo-reports/kvd105.

Goetz, S.C., F. Bangs, C.L. Barrington, N. Katsanis, and K.V. Anderson. 2017. The Meckel syndrome- associated protein MKS1 functionally interacts with components of the BBSome and IFT complexes to mediate ciliary trafficking and hedgehog signaling. *PLoS ONE*. 12:e0173399. doi:10.1371/journal.pone.0173399.

Gonçalves, J., and L. Pelletier. 2017. The Ciliary Transition Zone: Finding the Pieces and Assembling the Gate. *Mol. Cells*. 40:243–253. doi:10.14348/molcells.2017.0054.

Green, J.A., C.L. Schmid, E. Bley, P.C. Monsma, A. Brown, L.M. Bohn, and K. Mykytyn. 2015. Recruitment of β-Arrestin into Neuronal Cilia Modulates Somatostatin Receptor Subtype 3 Ciliary Localization. *Mol Cell Biol*. 36:223–235. doi:10.1128/MCB.00765-15.

Guadiana, S.M., S. Semple-Rowland, D. Daroszewski, I. Madorsky, J.J. Breunig, K. Mykytyn, and M.R. Sarkisian. 2013. Arborization of dendrites by developing neocortical neurons is dependent on primary cilia and type 3 adenylyl cyclase. *J Neurosci*. 33:2626–2638.

doi:10.1523/JNEUROSCI.2906-12.2013.

He, M., R. Subramanian, F. Bangs, T. Omelchenko, K.F. Liem, T.M. Kapoor, and K.V. Anderson. 2014. The kinesin-4 protein Kif7 regulates mammalian Hedgehog signalling by organizing the cilium tip compartment. *Nat Cell Biol.* 16:663–672. doi:10.1038/ncb2988.

Howarth, M., and A.Y. Ting. 2008. Imaging proteins in live mammalian cells with biotin ligase and monovalent streptavidin. *Nat Protoc.* 3:534–545. doi:10.1038/nprot.2008.20.

Hunnicutt, G.R., M.G. Kosfiszer, and W.J. Snell. 1990. Cell body and flagellar agglutinins in Chlamydomonas reinhardtii: the cell body plasma membrane is a reservoir for agglutinins whose migration to the flagella is regulated by a functional barrier. *J Cell Biol.* 111:1605–1616. doi:10.1083/jcb.111.4.1605.

Jackson, L.P., Owen, D.J., B.T. Kelly, A.J. Mccoy, T. Gaffry, L.C. James, B.M. Collins, S. Höning, and P.R. Evans. 2010. A large-scale conformational change couples membrane recruitment to cargo binding in the AP2 clathrin adaptor complex. *Cell.* 141:1220–1229. doi:10.1016/j.cell.2010.05.006.

Jensen, C.G., C.A. Poole, S.R. McGlashan, M. Marko, Z.I. Issa, K.V. Vujcich, and S.S. Bowser. 2004. Ultrastructural, tomographic and confocal imaging of the chondrocyte primary cilium in situ. *Cell Biol Int.* 28:101–110. doi:10.1016/j.cellbi.2003.11.007.

Jensen, V.L., and M.R. Leroux. 2017. Gates for soluble and membrane proteins, and two trafficking systems (IFT and LIFT), establish a dynamic ciliary signaling compartment. *Curr Opin Cell Biol.* 47:83–91. doi:10.1016/j.ceb.2017.03.012.

Jensen, V.L., C. Li, R.V. Bowie, L. Clarke, S. Mohan, O.E. Blacque, and M.R. Leroux. 2015. Formation of the transition zone by Mks5/Rpgrip1L establishes a ciliary zone of exclusion (CIZE) that compartmentalises ciliary signalling proteins and controls PIP2 ciliary abundance. *EMBO J.* 34:2537–2556. doi:10.15252/embj.201488044.

Jékely, G., and D. Arendt. 2006. Evolution of intraflagellar transport from coated vesicles and autogenous origin of the eukaryotic cilium. *Bioessays.* 28:191–198. doi:10.1002/bies.20369.

Jin, H., S.R. White, T. Shida, S. Schulz, M. Aguiar, S.P. Gygi, J.F. Bazan, and M.V. Nachury. 2010. The conserved Bardet-Biedl syndrome proteins assemble a coat that traffics membrane proteins to cilia. *Cell.* 141:1208–1219. doi:10.1016/j.cell.2010.05.015.

Kamachi, Y., and H. Kondoh. 1993. Overlapping positive and negative regulatory elements determine lens-specific activity of the delta 1-crystallin enhancer. *Mol Cell Biol.* 13:5206–5215.

Kanie, T., K.L. Abbott, N.A. Mooney, E.D. Plowey, J. Demeter, and P.K. Jackson. 2017. The CEP19-RABL2 GTPase Complex Binds IFT-B to Initiate Intraflagellar Transport at the Ciliary Base. *Dev Cell.* doi:10.1016/j.devcel.2017.05.016.

Kwon, R.Y., S. Temiyasathit, P. Tummala, C.C. Quah, and C.R. Jacobs. 2010. Primary cilium-

dependent mechanosensing is mediated by adenylyl cyclase 6 and cyclic AMP in bone cells. *FASEB J.* 24:2859–2868. doi:10.1096/fj.09-148007.

Lau, L., Y.L. Lee, S.J. Sahl, T. Stearns, and W.E. Moerner. 2012. STED microscopy with optimized labeling density reveals 9-fold arrangement of a centriole protein. *Biophys J.* 102:2926–2935. doi:10.1016/j.bpj.2012.05.015.

Lechtreck, K.F. 2015. IFT–Cargo Interactions and Protein Transport in Cilia. *Trends Biochem Sci.* 40:765–778. doi:10.1016/j.tibs.2015.09.003.

Lechtreck, K.F., E.C. Johnson, T. Sakai, D. Cochran, B.A. Ballif, J. Rush, G.J. Pazour, M. Ikebe, and G.B. Witman. 2009. The Chlamydomonas reinhardtii BBSome is an IFT cargo required for export of specific signaling proteins from flagella. *J Cell Biol.* 187:1117–1132. doi:10.1083/jcb.200909183.

Lechtreck, K.F., J.M. Brown, J.L. Sampaio, J.M. Craft, A. Shevchenko, J.E. Evans, and G.B. Witman. 2013. Cycling of the signaling protein phospholipase D through cilia requires the BBSome only for the export phase. *J Cell Biol.* 201:249–261. doi:10.1083/jcb.201207139.

Liem, K.F., M. He, P.J.R. Ocbina, and K.V. Anderson. 2009. Mouse Kif7/Costal2 is a cilia-associated protein that regulates Sonic hedgehog signaling. *Proc Natl Acad Sci U S A.* 106:13377–13382. doi:10.1073/pnas.0906944106.

Liew, G.M., F. Ye, A.R. Nager, J.P. Murphy, J.S. Lee, M. Aguiar, D. Breslow, S.P. Gygi, and M.V. Nachury. 2014. The intraflagellar transport protein IFT27 promotes BBSome exit from cilia through the GTPase ARL6/BBS3. *Dev Cell.* 31:265–278. doi:10.1016/j.devcel.2014.09.004.

Liu, Y.C., A.L. Couzens, A.R. Deshwar, L.D. B McBroom-Cerajewski, X. Zhang, V. Puviindran, I.C. Scott, A.-C. Gingras, C.-C. Hui, and S. Angers. 2014. The PPFIA1-PP2A protein complex promotes trafficking of Kif7 to the ciliary tip and Hedgehog signaling. *Science Signaling.* 7:ra117–ra117. doi:10.1126/scisignal.2005608.

Loktev, A.V., and P.K. Jackson. 2013. Neuropeptide Y family receptors traffic via the Bardet-Biedl syndrome pathway to signal in neuronal primary cilia. *Cell Rep.* 5:1316–1329. doi:10.1016/j.celrep.2013.11.011.

Mangeol, P., B. Prevo, and E.J.G. Peterman. 2016. KymographClear and KymographDirect: two tools for the automated quantitative analysis of molecular and cellular dynamics using kymographs. *Mol Biol Cell.* 27:1948–1957. doi:10.1091/mbc.E15-06-0404.

Masyuk, A.I., S.A. Gradilone, J.M. Banales, B.Q. Huang, T.V. Masyuk, S.-O. Lee, P.L. Splinter, A.J. Stroope, and N.F. LaRusso. 2008. Cholangiocyte primary cilia are chemosensory organelles that detect biliary nucleotides via P2Y12 purinergic receptors. 295:G725–G734. doi:10.1152/ajpgi.90265.2008.

Mick, D.U., R.B. Rodrigues, R.D. Leib, C.M. Adams, A.S. Chien, S.P. Gygi, and M.V. Nachury. 2015. Proteomics of Primary Cilia by Proximity Labeling. *Dev Cell.* 35:497–512.

doi:10.1016/j.devcel.2015.10.015.

Milenkovic, L., L.E. Weiss, J. Yoon, T.L. Roth, Y.S. Su, S.J. Sahl, M.P. Scott, and W.E. Moerner. 2015. Single-molecule imaging of Hedgehog pathway protein Smoothened in primary cilia reveals binding events regulated by Patched1. *Proc Natl Acad Sci U S A*. 112:8320–8325. doi:10.1073/pnas.1510094112.

Milenkovic, L., Milenkovic, L., M.P. Scott, M.P. Scott, and R. Rohatgi. 2009. Lateral transport of Smoothened from the plasma membrane to the membrane of the cilium. *J Cell Biol*. 187:365–374. doi:10.1083/jcb.200907126.

Moore, B.S., A.N. Stepanchick, P.H. Tewson, C.M. Hartle, J. Zhang, A.M. Quinn, T.E. Hughes, and T. Mirshahi. 2016. Cilia have high cAMP levels that are inhibited by Sonic Hedgehog-regulated calcium dynamics. *Proc Natl Acad Sci U S A*. 113:13069–13074. doi:10.1073/pnas.1602393113.

Morita, E., J. Arii, D. Christensen, J. Votteler, and W.I. Sundquist. 2012. Attenuated protein expression vectors for use in siRNA rescue experiments. *BioTechniques*. 0:1–5. doi:10.2144/000113909.

Mukhopadhyay, S., X. Wen, B. Chih, C.D. Nelson, W.S. Lane, S.J. Scales, and P.K. Jackson. 2010. TULP3 bridges the IFT-A complex and membrane phosphoinositides to promote trafficking of G protein-coupled receptors into primary cilia. *Genes Dev*. 24:2180–2193. doi:10.1101/gad.1966210.

Mukhopadhyay, S., X. Wen, N. Ratti, A. Loktev, L. Rangell, S.J. Scales, and P.K. Jackson. 2013. The ciliary G-protein-coupled receptor Gpr161 negatively regulates the Sonic hedgehog pathway via cAMP signaling. *Cell*. 152:210–223. doi:10.1016/j.cell.2012.12.026.

Nachury, M.V. 2008. Tandem affinity purification of the BBSome, a critical regulator of Rab8 in ciliogenesis. *Meth Enzymol*. 439:501–513. doi:10.1016/S0076-6879(07)00434-X.

Nachury, M.V., E.S. Seeley, and H. Jin. 2010. Trafficking to the ciliary membrane: how to get across the periciliary diffusion barrier? *Annu Rev Cell Dev Biol*. 26:59–87. doi:10.1146/annurev.cellbio.042308.113337.

Nager, A.R., J.S. Goldstein, V. Herranz-Pérez, D. Portran, F. Ye, J.M. García-Verdugo, and M.V. Nachury. 2017. An Actin Network Dispatches Ciliary GPCRs into Extracellular Vesicles to Modulate Signaling. *Cell*. 168:252–263.e14. doi:10.1016/j.cell.2016.11.036.

Ou, G., O.E. Blacque, J.J. Snow, M.R. Leroux, and J.M. Scholey. 2005. Functional coordination of intraflagellar transport motors. *Nature*. 436:583–587. doi:10.1038/nature03818.

Pal, K., S.-H. Hwang, B. Somatilaka, H. Badgandi, P.K. Jackson, K. DeFea, and S. Mukhopadhyay. 2016. Smoothened determines β-arrestin-mediated removal of the G protein-coupled receptor Gpr161 from the primary cilium. *J Cell Biol*. 212:861–875. doi:10.1083/jcb.201506132.

Prevo, B., P. Mangeol, F. Oswald, J.M. Scholey, and E.J.G. Peterman. 2015. Functional differentiation of cooperating kinesin-2 motors orchestrates cargo import and transport in C. elegans cilia. *Nat Cell Biol.* 17:1536–1545. doi:10.1038/ncb3263.

Putoux, A., S. Thomas, K.L.M. Coene, E.E. Davis, Y. Alanay, G. Ogur, E. Uz, D. Buzas, C. Gomes, S. Patrier, C.L. Bennett, N. Elkhartoufi, M.-H.S. Frison, L. Rigonnot, N. Joyé, S. Pruvost, G.E. Utine, K. Boduroglu, P. Nitschké, L. Fertitta, C. Thauvin-Robinet, A. Munnich, V. Cormier-Daire, R. Hennekam, E. Colin, N.A. Akarsu, C. Bole-Feysot, N. Cagnard, A. Schmitt, N. Goudin, S. Lyonnet, F. Encha-Razavi, J.-P. Siffroi, M. Winey, N. Katsanis, M. Gonzales, M. Vekemans, P.L. Beales, and T. Attié-Bitach. 2011. KIF7 mutations cause fetal hydrolethalus and acrocallosal syndromes. *Nat Genet.* 43:601–606. doi:10.1038/ng.826.

Rohrer, S.P., E.T. Birzin, R.T. Mosley, S.C. Berk, S.M. Hutchins, D.M. Shen, Y. Xiong, E.C. Hayes, R.M. Parmar, F. Foor, S.W. Mitra, S.J. Degrado, M. Shu, J.M. Klopp, S.J. Cai, A. Blake, W.W. Chan, A. Pasternak, L. Yang, A.A. Patchett, R.G. Smith, K.T. Chapman, and J.M. Schaeffer. 1998. Rapid identification of subtype-selective agonists of the somatostatin receptor through combinatorial chemistry. *Science.* 282:737–740. doi:10.1126/science.282.5389.737.

S.-H. Hwang, and S. Mukhopadhyay. 2017. Tubby family proteins are adapters for ciliary trafficking of integral membrane proteins. *J Cell Biol.* 216:743–760. doi:10.1083/jcb.201607095.

Sage, D., F.R. Neumann, F. Hediger, S.M. Gasser, and M. Unser. 2005. Automatic tracking of individual fluorescence particles: application to the study of chromosome dynamics. *IEEE Trans Image Process.* 14:1372–1383. doi:10.1109/TIP.2005.852787.

Shaner, N.C., G.G. Lambert, A. Chammas, Y. Ni, P.J. Cranfill, M.A. Baird, B.R. Sell, J.R. Allen, R.N. Day, M. Israelsson, M.W. Davidson, and J. Wang. 2013. A bright monomeric green fluorescent protein derived from Branchiostoma lanceolatum. *Nat Methods.* 10:407–409. doi:10.1038/nmeth.2413.

Shaner, N.C., R.E. Campbell, P.A. Steinbach, B.N.G. Giepmans, A.E. Palmer, and R.Y. Tsien. 2004. Improved monomeric red, orange and yellow fluorescent proteins derived from Discosoma sp. red fluorescent protein. *Nat Biotechnol.* 22:1567–1572. doi:10.1038/nbt1037.

Shen, F., L. Cheng, A.E. Douglas, N.A. Riobo, and D.R. Manning. 2013. Smoothened is a fully competent activator of the heterotrimeric G protein G(i). *Molecular Pharmacology.* 83:691–697. doi:10.1124/mol.112.082511.

Su, X., K. Driscoll, G. Yao, A. Raed, M. Wu, P.L. Beales, and J. Zhou. 2014. Bardet-Biedl syndrome proteins 1 and 3 regulate the ciliary trafficking of polycystic kidney disease 1 protein. *Hum Mol Genet.* 23:5441–5451. doi:10.1093/hmg/ddu267.

Trimble, W.S., and S. Grinstein. 2015. Barriers to the free diffusion of proteins and lipids in the plasma membrane. *J Cell Biol.* 208:259–271. doi:10.1083/jcb.201410071.

van Dam, T.J.P., M.J. Townsend, M. Turk, A. Schlessinger, A. Sali, M.C. Field, and M.A. Huynen. 2013. Evolution of modular intraflagellar transport from a coatomer-like progenitor. *Proc Natl Acad Sci U S A*. 110:6943–6948. doi:10.1073/pnas.1221011110.

Williams, C.L., J.C. McIntyre, S.R. Norris, P.M. Jenkins, L. Zhang, Q. Pei, K. Verhey, and J.R. Martens. 2014. Direct evidence for BBSome-associated intraflagellar transport reveals distinct properties of native mammalian cilia. *Nature Communications*. 5:5813. doi:10.1038/ncomms6813.

Yang, T.T., J. Su, W.-J. Wang, B. Craige, G.B. Witman, M.-F.B. Tsou, and J.C. Liao. 2015. Superresolution Pattern Recognition Reveals the Architectural Map of the Ciliary Transition Zone. *Sci Rep*. 5:14096. doi:10.1038/srep14096.

Yasuda, K., S. Rens-Domiano, C.D. Breder, S.F. Law, C.B. Saper, T. Reisine, and G.I. Bell. 1992. Cloning of a novel somatostatin receptor, SSTR3, coupled to adenylylcyclase. *J Biol Chem*. 267:20422–20428.

Ye, F., D. Breslow, E.F. Koslover, A.J. Spakowitz, W.J. Nelson, and M.V. Nachury. 2013. Single molecule imaging reveals a major role for diffusion in the exploration of ciliary space by signaling receptors. *Elife*. 2:e00654. doi:10.7554/eLife.00654.

Yee, L.E., F.R. Garcia-Gonzalo, R.V. Bowie, C. Li, J.K. Kennedy, K. Ashrafi, O.E. Blacque, M.R. Leroux, and J.F. Reiter. 2015. Conserved Genetic Interactions between Ciliopathy Complexes Cooperatively Support Ciliogenesis and Ciliary Signaling. *PLoS Genet*. 11:e1005627. doi:10.1371/journal.pgen.1005627.

Yeh, C., A. Li, J.Z. Chuang, M. Saito, A. Caceres, and C.H. Sung. 2013. IGF-1 activates a cilium-localized noncanonical Gβγ signaling pathway that regulates cell-cycle progression. *Dev Cell*. 26:358–368. doi:10.1016/j.devcel.2013.07.014.

Zhang, Q., D. Nishimura, S. Seo, T. Vogel, D.A. Morgan, C. Searby, K. Bugge, E.M. Stone, K. Rahmouni, and V.C. Sheffield. 2011. Bardet-Biedl syndrome 3 (Bbs3) knockout mouse model reveals common BBS-associated phenotypes and Bbs3 unique phenotypes. *Proc Natl Acad Sci U S A*. 108:20678–20683. doi:10.1073/pnas.1113220108.

Zhang, Q., S. Seo, K. Bugge, E.M. Stone, and V.C. Sheffield. 2012. BBS proteins interact genetically with the IFT pathway to influence SHH-related phenotypes. *Hum Mol Genet*. 21:1945–1953. doi:10.1093/hmg/dds004.

Zhang, Y., S. Seo, S. Bhattarai, K. Bugge, C.C. Searby, Q. Zhang, A.V. Drack, E.M. Stone, and V.C. Sheffield. 2014. BBS mutations modify phenotypic expression of CEP290-related ciliopathies. *Hum Mol Genet*. 23:40–51. doi:10.1093/hmg/ddt394.

Acknowledgments:

We thank Drs. M. Bornens for the Ninein antibody, S. Saunier for the Cep290 antibody, T. Stearns for the Cep164 antibody, K. Anderson for the Kif7 cDNA, S. Mukhopadhyay for the GPR161 antibody, P. Beachy for the δ-crystallin promoter, J. Eggenschweiler for the Tulp3 antibody, C. Smith for the BBS5 monoclonal antibody, M. Lin for neurons, T. Gadella for mScarlet cDNA, Novartis for ACQ090, and Mr. A. Kopp and Ms. J. Goldstein for technical assistance. We thank Drs. K. Hill, A. Benmerah and the Nachury lab for comments on the manuscript. This work was supported by NIH funding (GM089933 to M.V.N) and a Fayez Sarofim/Damon Runyon Fellowship to A.R.N. (DRG 2160-13). M.V.N. conceived and coordinated the project and wrote the paper with contributions from all authors; F.Y. and A.R.N jointly developed the cell lines used for imaging of GPCRs and BBSome; F.Y. conducted all single-molecule imaging and the quantitative analysis of BBSome trains and exit. Data described can be found in the main figures and supplementary materials. The authors declare no conflict of interest.

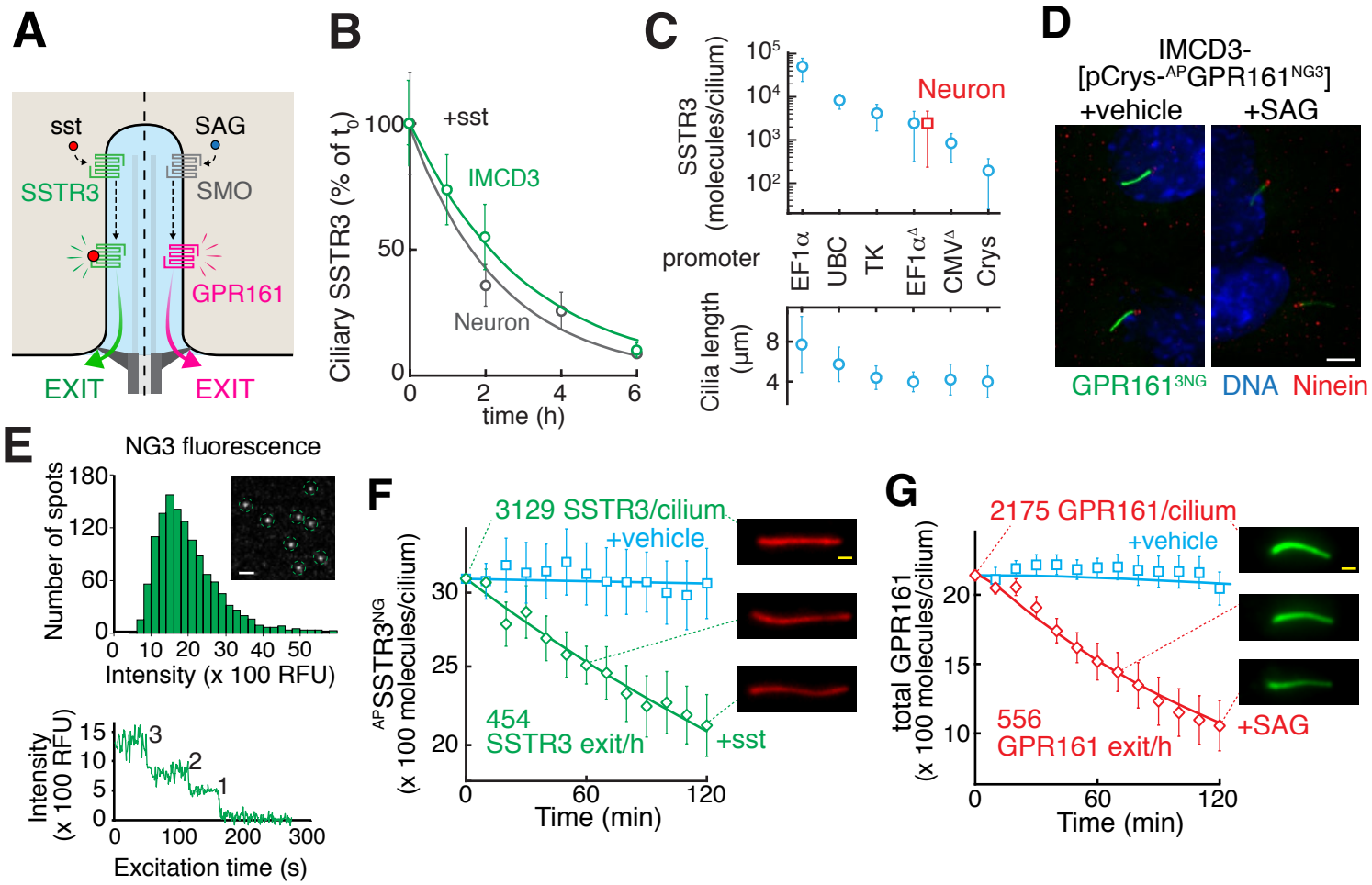

Ye et al., Figure 1

Figure 1. Reconstitution of signal-dependent retrieval of SSTR3 and GPR161

(**A**) Diagram of the signal-dependent retrieval systems under study. Left: addition of somatostatin triggers SSTR3 exit from cilia by directly activating SSTR3. Right: addition of Smoothened agonist (SAG) activates the Hedgehog pathway and promotes GPR161 retrieval. (**B**) Kinetics of SSTR3 disappearance from cilia of primary hippocampal neurons and of IMCD3 stably expressing ^{AP}SSTR3^{NG} under the control of the TATA-less EF1α promoter were estimated by quantitation of immunofluorescence signals following addition of sst. The entire data set for the sst condition is shown in Fig. **S1B**. Data were fitted to a single exponential. Error bars: 95% CI. N = 280-424 cilia (neurons), 57-80 cilia (IMCD3). (**C**) High level expression of SSTR3 drives elongation of primary cilia. Top: ^{AP}SSTR3^{GFP} driven by various promoters was expressed stably at the FlpIn locus of IMCD3 cells and ciliary GFP levels were measured and compared to a GFP calibrator (Breslow et al., 2013). Endogenous SSTR3 levels were estimated by comparative immunostaining (see Methods), N = 10-38 cilia. Error bars: SD. Bottom: Effect of ^{AP}SSTR3^{GFP} expression on cilium length. Cilia lengths were measured in the GFP channel by live-cell imaging. Error bars represent SD, N = 10-38 cilia. Cilium lengthening upon GPCR overexpression was previously reported by (Guadiana et al., 2013). (**D**) IMCD3-[pCrys-^{AP}GPR161^{3NG}] were treated for 2 h with either SAG or vehicle. ^{AP}GPR161^{3NG} was visualized by NG fluorescence, basal bodies of cilia stained with Ninein. All cells were pre-treated with the translation inhibitor emetine to eliminate signals from new protein synthesis. Scale bar: 4 µm. (**E**) Absolute quantitation of ciliary GPCR abundance. Top: Calibration of single molecule fluorescence intensity. Bacterially expressed triple NeonGreen (NG3) protein was spotted on glass coverslips (inset) and the fluorescent intensity of each individual NG3 was measured. N = 1257 particles measured. Bottom: The 3-step photobleaching of a representative spot shows that the fluorescence was emitted by a single NG3 molecule. The measured fluorescence intensity of NG3 was used to calibrate NG- and NG3-tagged SSTR3, GPR161, BBS5 and IFT88. (**F**) IMCD3-[pEF1α$^{\Delta}$-^{AP}SSTR3^{NG}] cells were treated with vehicle or sst for 2h. Stable expression of an ER-localized biotin ligase BirA enables detection of ^{AP}SSTR3 by pulse-labeling live cells with Alexa647-conjugated mSA (mSA647) and tracking individual cilia. The absolute number of ^{AP}SSTR3^{NG} molecules per cilia at t_0 was calculated by measuring the NG signal and using the NG3 calibrator. For all other time points, the ratio in ciliary mSA647 signal compared to t_0 was used to calculate the absolute number of molecules (see Methods for details). Data were fitted to a single exponential. Error bars: 95% CI. N = 14 cilia. (**G**) IMCD3-[pCrys-GPR161^{3NG}] cells were treated with SAG or vehicle for 2h. NG fluorescence was tracked in individual cilia and the ratio of GPR161^{3NG} to endogenous GPR161 was used to calculate the total levels of GPR161. Data were fitted to a single exponential. Error bars: 95% CI. N =12-20 cilia.

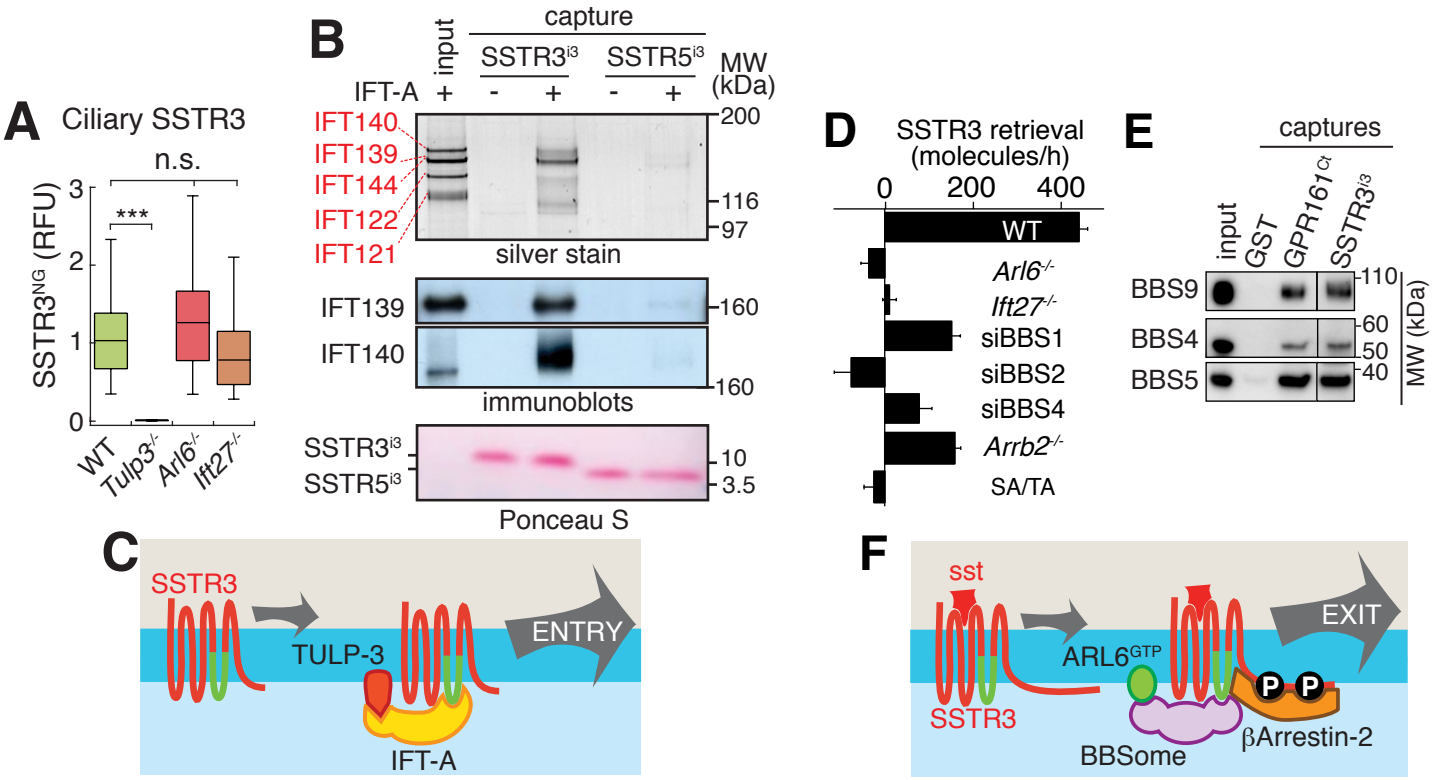

Ye et al., Figure 2

Figure 2. Roles of IFT-A and BBSome in ciliary entry and exit.
(**A**) Tulp3 is required for ciliary entry of SSTR3. Box plots of ciliary ^{AP}SSTR3^{NG} intensities measured by NG fluorescence (Relative Fluorescent Unit, RFU) for various IMCD3 lines. *Tulp3*$^{-/-}$ cells were fixed to identify cilia using anti-acetylated tubulin staining, all other cells were imaged live as cilia were readily identified in the NG channel. NG fluorescence was not affected by fixation (Fig. **S2B**). Asterisks indicate ANOVA significance values; *** $P < 10^{-4}$, n.s. $P > 0.05$. N = 18-59 cilia. (**B**) IFT-A directly recognizes SSTR3^{i3}. The IFT-A complex nwas purified from IMCD3-[LAP-IFT43] cells and incubated with beads coated with GST-SSTR3^{i3} or GST-SSTR5^{i3}. Captured materials were eluted by cleaving off the beads and visualized by silver stain and immunoblotting. 5 input equivalents were loaded in the eluate lanes. (**F**) Model of ciliary entry. (**D**) BBSome subunits were depleted by siRNA, *Arl6*, *Ift27* and *β-arrestin 2* (*Arrb2*) genes were knocked out by genome editing and SA/TA denotes a phosphomutant of the C-tail of SSTR3 that is unable to bind to β-arrestin 2. Absolute retrieval rates were calculated by linear fitting of retrieval kinetics (see (Nager et al., 2017)). Error bars: error of the fit. N =10-35 cilia. (**E**) BBSome purified to near-homogeneity from bovine retina was incubated with glutathione beads coated with GST, GST-GPR161^{Ct} and GST-SSTR3^{i3}. Captured materials were cleavage-eluted and immunoblotted. 3 input equivalents were loaded in the eluate lanes. (**F**) Signal-dependent retrieval requires the joint activities of Arl6-GTP, BBSome and β-arrestin 2.

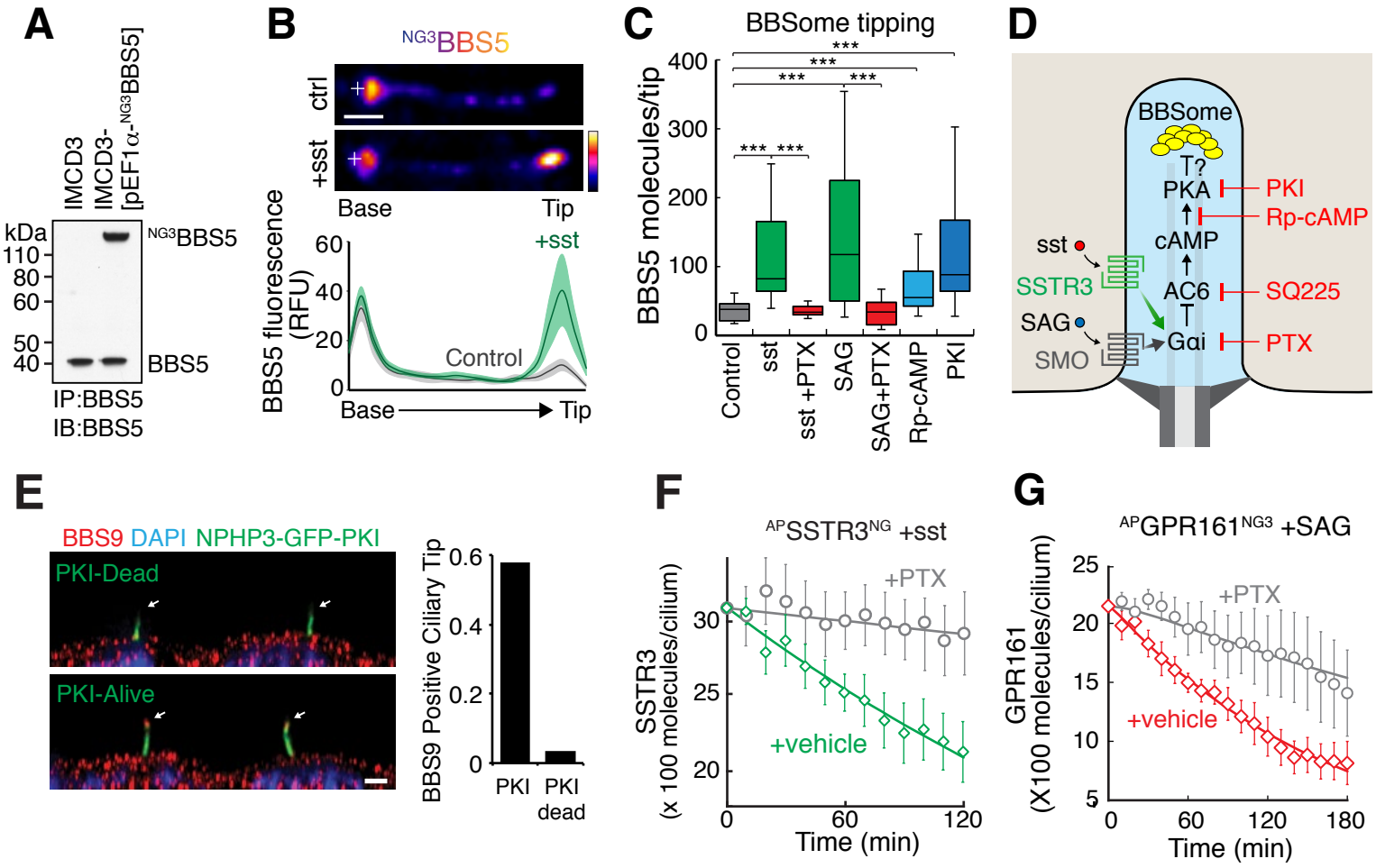

Ye et al., Figure 3

Figure 3. A Gαi-PKA axis promotes BBSome tip accumulation and GPCR retrieval.
(**A**) Near endogenous expression of ^{NG3}BBS5. IMCD3 and IMCD3-[pEF1α-^{NG3}BBS5] cells were subjected to immunoprecipitation with an anti-BBS5 antibody and lysates and eluates were immunoblotted for BBS5. Molecular weights (kDa) are indicated on the right. Measurement of band intensities with Image Lab (Bio-Rad) indicates that the molar ratios between ^{NG3}BBS5 and endogenous BBS5 is 1.27. (**B**) IMCD3-[pEF1α$^{\Delta}$-^{AP}SSTR3, pEF1α-^{NG3}BBS5] were treated with sst or vehicle for 40 min. Top: Representative images of cilia from live cells. ^{NG3}BBS5 is in fire scale and a white cross marks the location of the basal body (see **S2J**). Bottom: line scans of ^{NG3}BBS5 fluorescence intensities along cilia of live cells. The line marks the average intensity along length-normalized cilia. The shaded area shows the 95% confidence interval. N = 20-29 cilia. Scale bar: 1 µm. (**C**) ^{NG3}BBS5 tip fluorescence was quantified in live cells after 40 min of incubation with sst, SAG, Rp-cAMPs or PKI. Cells were pre-incubated with Pertussis toxin (PTX) for 16 h to fully inactivate $G\alpha_i$. The total number of BBS5 molecules at the tip was calculated using the NG3 calibrator and the measured ratio of ^{NG3}BBS5 to total BBS5. The whiskers represent 1.5x the interquartile range. Asterisks indicate Mann Whitney test significance values; *** $P < 0.0005$. N = 20-29 cilia from 3 independent experiments. (**D**) The pathways downstream of Smoothened (SMO) and SSTR3 and the site of action of the pharmacological perturbations are shown. (**E**) Representative immunofluorescence images of ciliary BBS9 (red) in IMCD3-[pEF1α-NPHP3$^{GFP\text{-}PKI}$] and IMCD3-[pEF1α-NPHP3$^{GFP\text{-}PKIdead}$] cells (Mick et al., 2015). Optical sections were deconvolved and X-Z projections are shown. Arrows mark the tips of cilia. The numbers of ciliary tips positive for BBS9 are plotted in the right panel. Scale bar: 2 µm. (**F-G**) Pertussis toxin slows down the exit of SSTR3 (**F**) and GPR161 (**G**). IMCD3-[pEF1α$^{\Delta}$-^{AP}SSTR3^{NG}] or IMCD3-[pCrys-^{AP}GPR161^{3NG}] were pre-treated with PTX for 16 h to fully inactivate $G\alpha_i$. After agonist treatment, ciliary GPCR levels were measured in live cells as described in Fig. **1F-G**. Error bars: 95% CI. N = 10-28 cilia. (**H-I**) PKA inhibition accelerates the exit of SSTR3 (**H**) and GPR161 (**G**). IMCD3-[pEF1α$^{\Delta}$-^{AP}SSTR3^{NG}] or IMCD3-[pCrys-^{AP}GPR161^{3NG}] cells were treated for 3 h with the indicated concentrations of agonist and/or PKI. Ciliary level of GPCRs were measured by NeonGreen fluorescence before and after treatment to estimate the rate of exit. Addition of PKI together with sub-saturating concentrations of agonist significantly accelerated the GPCR exit rates to the near-maximal values observed with saturating concentrations of agonist. Error bars: Error of the fit. N = 67-112 cilia from 3 independent experiments. Asterisks indicate multiple regression significance values; *$P < 0.05$.

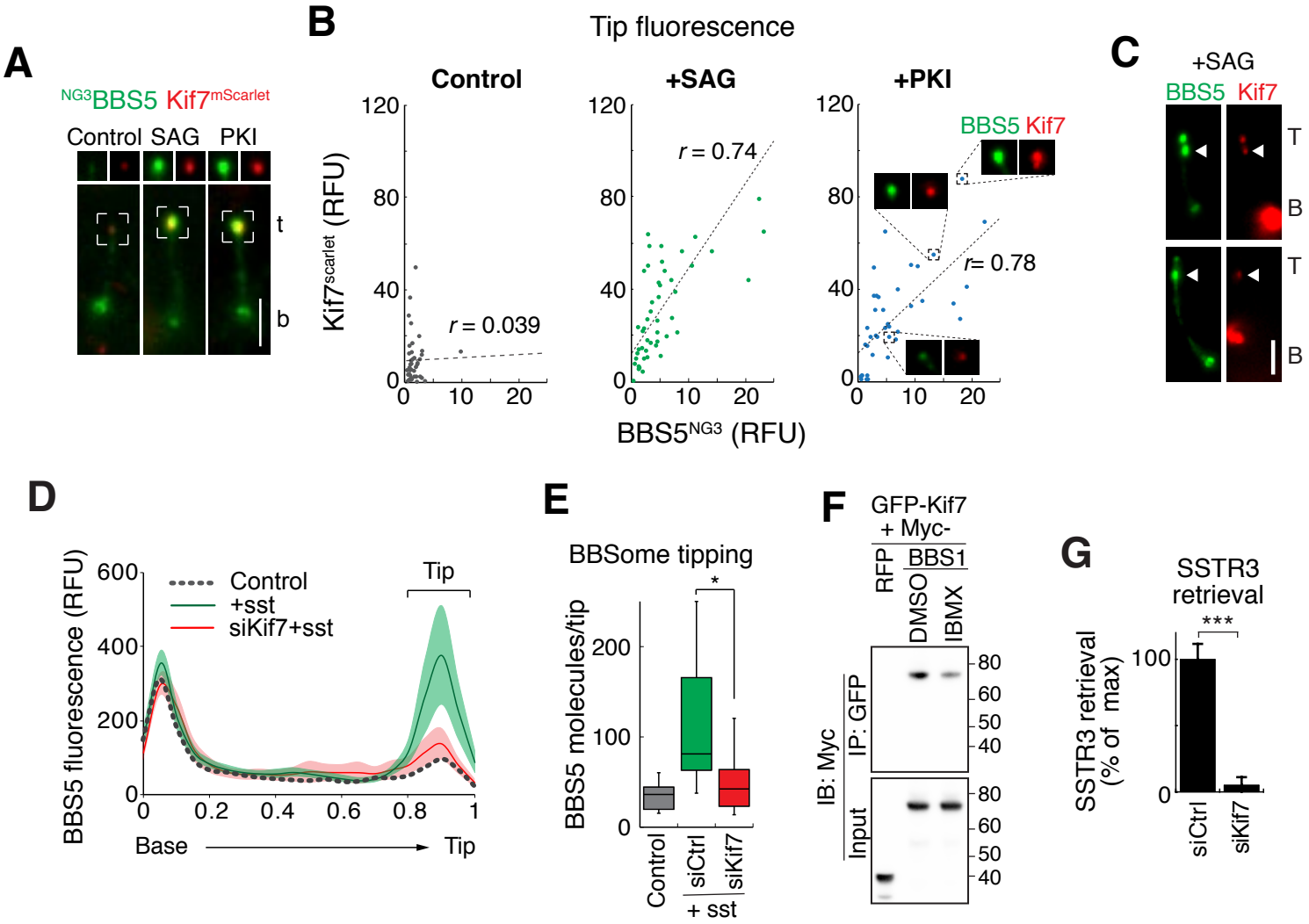

Ye et al., Figure 4

Figure 4. PKA antagonizes the recruitment of the BBSome to the tip of cilia by Kif7
(**A-C**) Co-recruitment of BBS5 and Kif7 to the tip of cilia in live IMCD3-[pEF1α-^{NG3}BBS5; pCMV-Kif7^{mScarlet}] cells. (**A**) Representative images showing SAG- and PKI-induced accumulation of ^{NG3}BBS5 and Kif7^{mScarlet} at ciliary tip. Cells were treated with SAG, PKI or vehicle for 40 min before imaging. White boxes mark the ciliary tip and split channels of ^{NG3}BBS5 and Kif7^{mScarlet} are shown on top. Scale bar: 2 µm. (**B**) Correlation between the fluorescence signal of ^{NG3}BBS5 and Kif7^{Scarlet} at the ciliary. Fluorescence signals of ^{NG3}BBS5 and Kif7^{mScarlet} were measured at ciliary tip of live cells after 40 min treatment with vehicle, SAG or PKI. Micrographs of ^{NG3}BBS5 and Kif7^{mScarlet} at the ciliary tip for three representative data points are shown. Linear regressions (dotted lines) highlight the positive correlation between ciliary tip levels of ^{NG3}BBS5 and Kif7^{mScarlet} in the presence of SAG or PKI The Pearson correlation coefficient (r) is shown. N =40-49 cilia. (**C**) In SAG-treated cells where a second spot of Kif7 is occasionally found along cilia, a second spot of BBS5 was observed at the same location as Kif7. The white arrowheads mark the location of ^{NG3}BBS5 foci that accumulated at the ectopic tip. Scale bar: 2 µm. (**D-E**) Kif7 is necessary for the redistribution of BBS5 to the tip of cilia. (**D**) Linescans of ^{NG3}BBS5 fluorescence intensities along cilia of live cells. Cells were transfected with siRNAs for 72h and treated with sst for 40 min before live imaging of ^{NG3}BBS5 fluorescence. The line marks the average intensity along length-normalized cilia. The shaded areas show the 95% confidence interval (not shown for the vehicle control). N = 20-27 cilia. (**E**) The total number of BBS5 molecules at the tip was calculated as in Fig. **3C**. Asterisks indicate Mann Whitney test significance values; * $P < 0.05$. N = 20-28 cilia from 3 independent experiments. (**F**) Kif7 interacts with BBSome and PKA antagonizes this interaction. HEK293 cells co-transfected with Kif7^{GFP} and ^{Myc}BBS1 were treated with the cAMP phosphodiesterase inhibitor IBMX or vehicle for 30 min before lysis. Complexes were immunoprecipitated with anti-GFP antibodies. Lysates and eluates were blotted for Myc. The capture efficiency of ^{Myc}BBS1 by Kif7^{GFP} was decreased 29 ± 3% upon treatment with IBMX. Molecular weights (kDa) are indicated on the right. N = 3 independent experiments. (**G**) Kif7 is necessary for SSTR3 exit from cilia. IMCD3-[^{AP}SSTR3^{NG}] cells were treated with siRNA targeting Kif7 or Luciferase, pulse-labeled with SA647, and imaged every 10 min following addition of sst. The resulting loss in SA647 fluorescence was plotted and linearly fitted to determine the rate of SSTR3 retrieval. Asterisks indicate Mann Whitney test significance values; *** $P <$ 0.0005. Error bars: SD. (n=13 cilia)

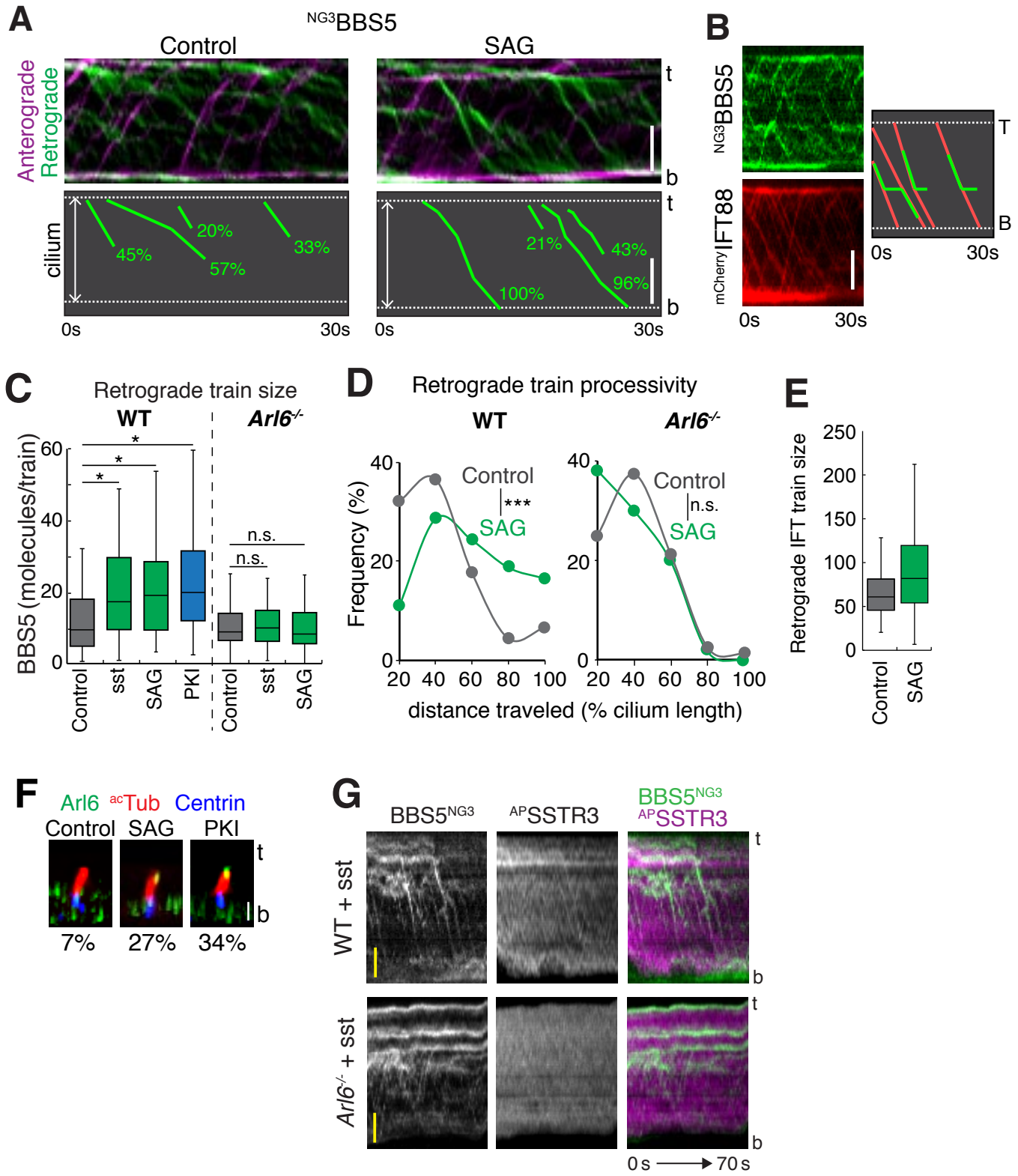

Ye et al., Figure 5

Figure 5. GPCR signaling and Arl6 drive assembly of large, processive retrograde BBSome trains.

(**A**) Representative kymographs from IMCD3-[pEF1α-^{NG3}BBS5] cells treated with SAG or vehicle for 40 min before imaging at 4 Hz for 30 s. Kymographs were deconvolved into anterograde (magenta) and retrograde (green) components (see methods). The distance traveled by each retrograde train (normalized to the length of cilia) is indicated in the bottom diagram. Scale bar: 2 µm. t: tip, b: base. (**B**) Representative kymograph from an IMCD3-[pEF1α-^{NG3}BBS5, pCMV-^{mcherry}IFT88] cell showing the co-movement and the uncoupling between IFT-B and BBSome trains. (**C-D**) WT or *Arl6*$^{-/-}$ IMCD3-[pEF1α-^{NG3}BBS5; pEF1α$^{\Delta}$-^{AP}SSTR3] cells were treated with vehicle, sst, SAG or PKI for 40 min before imaging. (**C**) The processivity of retrograde BBSome trains was assessed as in (**A**). N = 52-91 cilia form 3 independent experiments. Asterisks indicate the significance values of Mann-Whitney U test applied to the entire distribution; *** $P < 0.0005$, n.s. $P > 0.05$. (**D**) The fluorescence intensity of ^{NG3}BBS5 retrograde trains was extracted from deconvolved kymographs and the total number of BBS5 molecules per train was calculated (see methods). The whiskers represent 1.5x the interquartile range. N = 52-91 cilia from 3 independent experiments. Asterisks indicate Mann-Whitney U test significance values; *** $P < 10^{-4}$, n.s. $P > 0.05$. (**E**) The number of IFT88 molecules per retrograde train was measured in IMCD3-[pEF1α-^{NG3}IFT88] cells treated with vehicle or SAG. Counting of molecules is detailed in Methods. (**F**) Arl6 immunofluorescence of cells treated with vehicle, SAG or PKI. Optical sections were deconvolved and X-Z projections are shown. The percentages of Arl6-positive tips are indicated below the micrographs. N = 88-118 cilia from 4 to 5 microscopic fields. (**G**) Representative kymographs from mSA647-labeled WT or *Arl6*$^{-/-}$ IMCD3-[pEF1α-^{NG3}BBS5; pEF1α$^{\Delta}$-^{AP}SSTR3] cells treated with sst for 1 h before imaging. The cells stably expressed an ER-localized biotin ligase BirA to enable visualization of ^{AP}SSTR3 by mSA647 labeling.

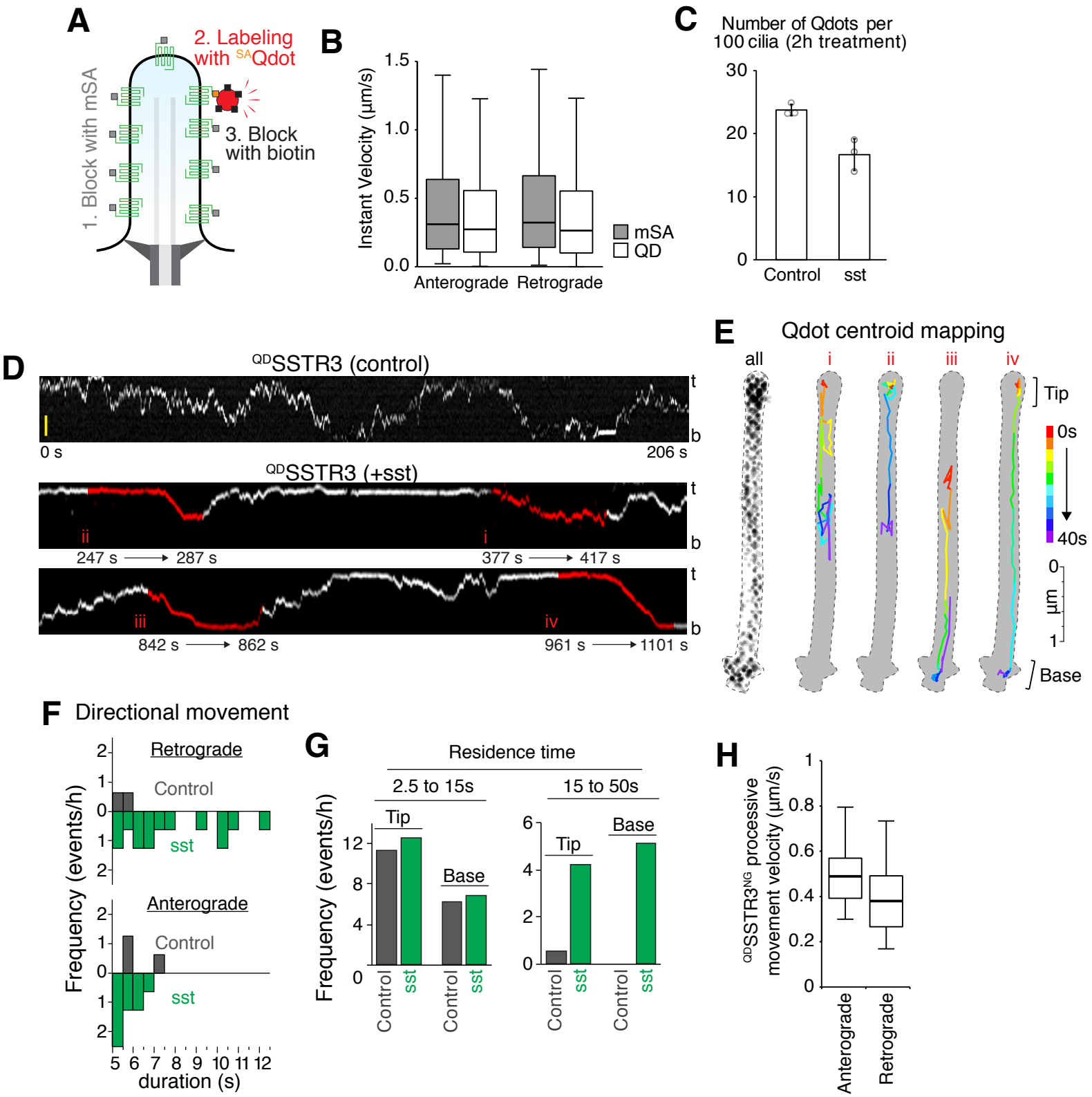

Ye et al., Figure 6

Figure 6. Activated GPCRs undergo processive retrograde movements, and confinements at base and tip

(**A**) Diagram of the Qdot labeling strategy. IMCD3-[pEF1α^{A}-^{AP}SSTR3^{NG}] cells stably expressing BirA-ER were first treated with unlabeled mSA to passivate the surface-exposed biotinylated ^{AP}SSTR3. ^{SA}Qdots were then added to the medium to label the GPCRs newly arrived at the surface. Finally, biotin was added to the medium to passivate the excess SA on Qdots. (**B**) The diffusive properties of SSTR3 are not altered by QDFot labeling. The instantaneous velocities of mSA647-labeled ^{AP}SSTR3^{NG} and QDot655-labeled ^{AP}SSTR3^{NG} were measured by single molecule tracking in the absence of sst. Error bars: SEM. (**C**) Qdot labeling does not alter the exit rate of SSTR3. IMCD3-[pEF1α-^{AP}SSTR3^{GFP}] cells were sparsely labeled with Qdot655 as described in Methods and treated with vehicle or sst for 2h before fixation. The number of Qdot per cilium was counted in both vehicle or sst treated condition. N = 263-303 cilia from three independent experiments. Error bars: SEM. (**D**) Representative kymographs showing the movements of ^{SA}Qdot-labeled ciliary ^{AP}SSTR3^{NG} (^{QD}SSTR3) in vehicle- or sst-treated cells. Red labels and line coloring highlight four characteristic movement behaviors. Scale bar: 2 μm. (**E**) Centroid mapping of ^{QD}SSTR3. Left: the contour of the cilium was traced as a dotted line that captures all ^{QD}SSTR3 positions. (i) diffusive movement, (ii) tip confinement followed by retrograde movement, (iii) retrograde movement followed by base confinement and return into the cilium, and (iv) tip confinement followed by fully processive retrograde movement and base confinement. The time dimension is color-coded from red to purple. (**F-G**) Signaling increases tip confinement and processive retrograde movement of SSTR3. Cells were treated with sst (green, sst) or vehicle (grey, Control) for 40 min before imaging was initiated for 10 to 20 min. (**F**) Durations of persistent movement events for ^{QD}SSTR3 in anterograde and retrograde directions. (**G**) The durations of confinement events for ^{QD}SSTR3 at ciliary tip or base were binned into two categories. N =12 cilia for each condition. (**H**) Velocities of persistent movements of ^{QD}SSTR3 after sst treatment. Error bars: SD

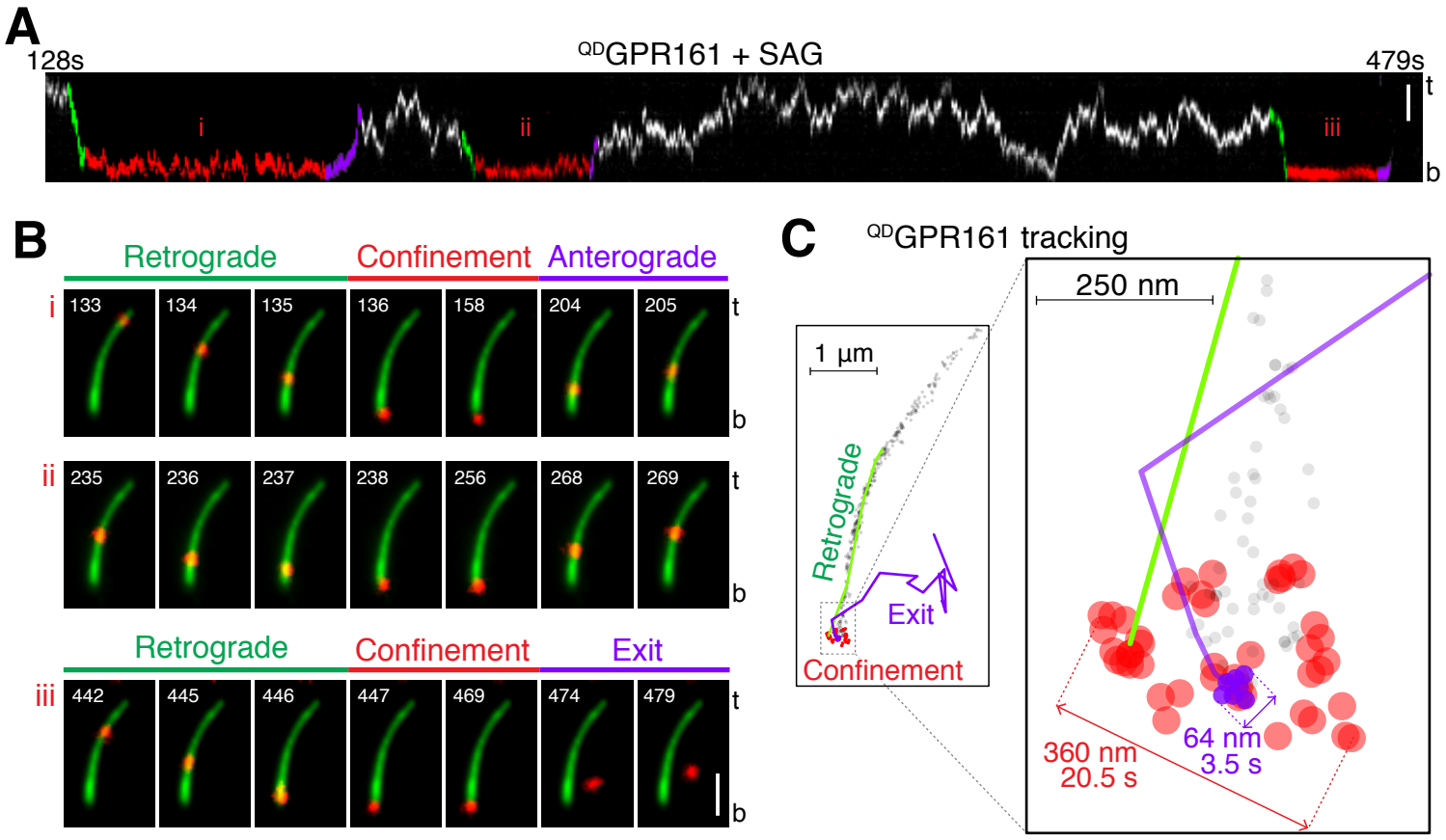

Ye et al., Figure 7

Figure 7. GPCR base confinement results in either exit or re-entry
(**A**) Cilium kymograph of ^{QD}GPR161. Cells were treated with SAG for 40 min before the start of imaging. Green, red and purple labels and line coloring indicate retrograde movements, confinement and anterograde transport (events i and ii) or exit from cilia (iii). Scale bar: 2 µm. (**B**) Time series of the three confinement events. A reference image of bulk NG fluorescence from ^{AP}GPR161^{NG3} was overlaid with images of ^{QD}GPR161. Time stamp (s) is in the upper left corner. Scale bar: 2 µm. t: tip. b: base. (**C**) Centroid mapping of ^{QD}GPR161 during event iii. The ^{QD}GPR161 locations captured during the entire imaging session are shown as grey dots. The green track represents a processive retrograde transport event that precedes confinement of ^{QD}GPR161 (shown in red dots) at the base. Immediately before diffusion away from the cilium (purple track), ^{QD}GPR161 was nearly immobile for 4.5 s (purple dots).

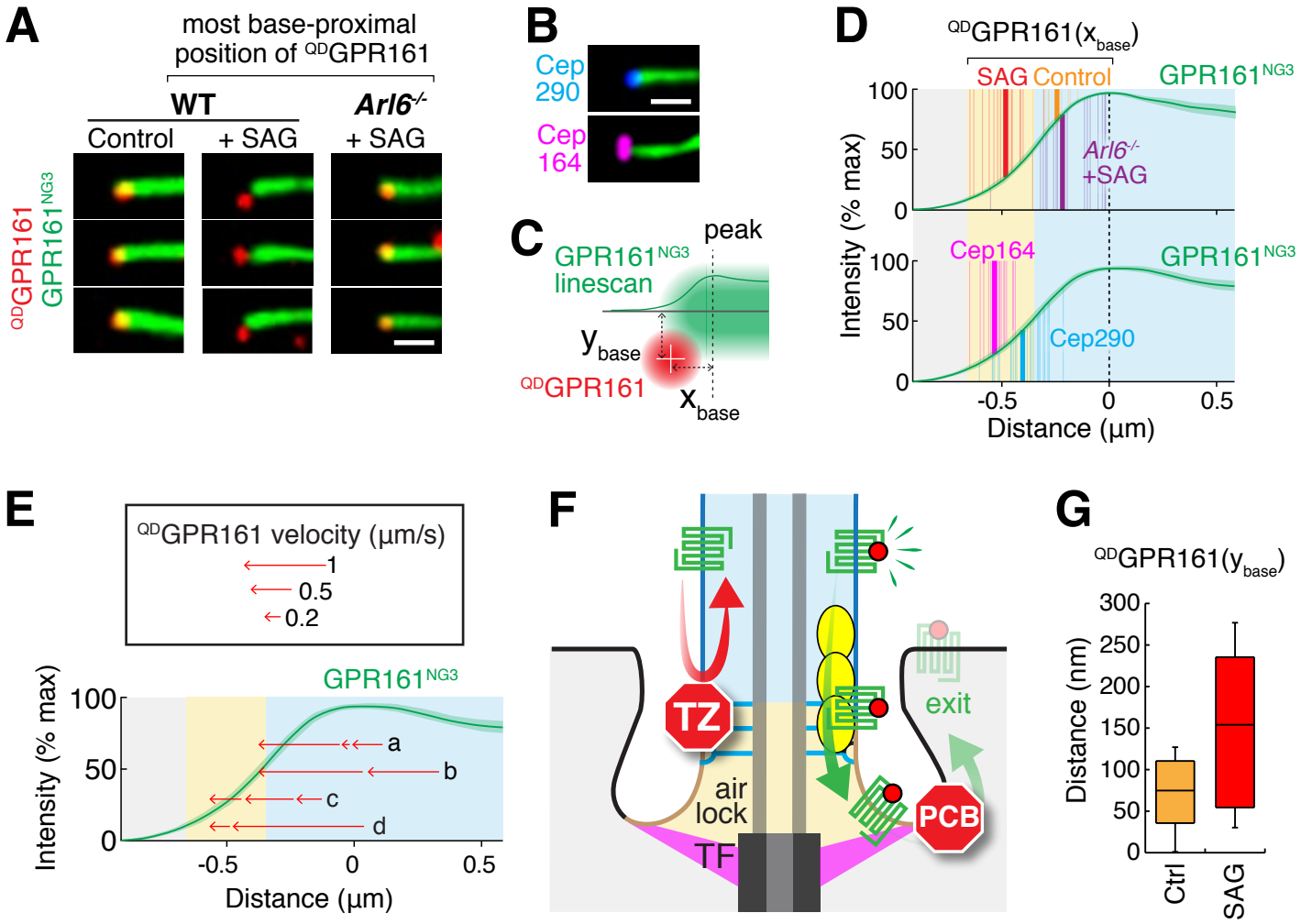

Ye et al., Figure 8

Figure 8. GPR161 traverses the transition zone in an Arl6- and signaling-dependent manner

(**A**) Representative images of the most base-proximal position of ^{QD}GPR161 (red) relative to bulk ^{AP}GPR161^{NG3} fluorescence (green) in WT or *Arl6*$^{-/-}$ IMCD3 cells treated with SAG or vehicle for 40 min before imaging. (**B**) Immunofluorescence staining of Cep164 (magenta) and Cep290 (blue). ^{AP}GPR161^{NG3} was visualized directly by NG fluorescence (bottom). Scale bar: 1 µm. (**C**) Diagram illustrating 2D mapping of the Qdot centroid relative to the bulk fluorescence of ^{AP}GPR161^{NG3}. (**D**) Longitudinal scans of ^{AP}GPR161^{NG3} fluorescence were used as references to map the most base-proximal positions of ^{QD}GPR161 (top) and the peaks of Cep164 and Cep290 signals in immunofluorescence images (bottom). Individual data points were plotted as thin vertical lines and the means plotted as thick lines. The longitudinal pattern of ^{AP}GPR161^{NG3} fluorescence is unchanged by fixation (Fig. **S5C**) thus enabling the use of the peak of fluorescence as a reference location to align the positions of ^{QD}GPR161, Cep290 and Cep164. The airlock is displayed in tan color, the cilium shaft is blue and the cell is gray. Error range (green shading): 95% CI. N = 15-26. (**E**) Instant velocities of ^{QD}GPR161 moving in a processive retrograde manner into the airlock. The four events are boxed in Fig. **S4D**. (**F**) Two-barrier model for exit from cilia. The background color scheme is as in (D). GPCR is green, agonist is red, BBSome/Arl6 coats are yellow. TF: transition fibers, TZ: transition zone, PCB: periciliary barrier. (**G**) Lateral displacement of ^{QD}GPR161 from the main axis of cilia during airlock visits. The y coordinates of the ^{QD}GPR161 positions extracted in (D) were mapped as shown in (C). N = 11-16 cilia.